

JPRS-UPM-91-004

6 JUNE 1991

Foreign
Broadcast
Information
Service



A N N I V E R S A R Y
1 9 4 1 - 1 9 9 1

JPRS Report

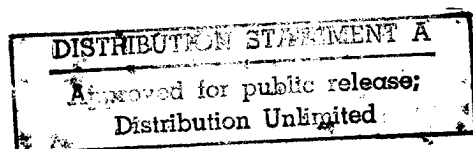
Science & Technology

USSR: Physics & Mathematics

19990305 052

DTIC QUALITY INSPECTED 3

REPRODUCED BY
U.S. DEPARTMENT OF COMMERCE
NATIONAL TECHNICAL INFORMATION SERVICE
SPRINGFIELD, VA. 22161



Science & Technology

USSR: PHYSICS & MATHEMATICS

JPRS-UPM-91-004

CONTENTS

6 JUNE 1991

ACOUSTICS

Observation of Standing Surface Acoustic Waves in Crystals by Methods of X-Ray Topography [O. P. Aleshko-Ozhevskiy, A. S. Pogosyan, et al.; <i>PISMA V ZHURNAL TEKHNIЧЕСКОY FIZIKI</i> Vol 16 No 17, 12 Sep 90]	1
Processing and Interpretation of Experimental Data on Microwave Interferometry of Shock Waves in Weakly Ionized Plasma [A. P. Yershov, S. V. Klishin, et al.; <i>TEPLOFIZIKA VYSOKIKH TEMPERATUR</i> Vol 28 No 6, Nov-Dec 90] ..	1
Peculiarities and Time Characteristics of Radiation Emission by Plasma Shock-Injected Into Air [A. F. Aleksandrov, K. Sh. Isayev, et al.; <i>TEPLOFIZIKA VYSOKIKH TEMPERATUR</i> Vol 28 No 6, Nov-Dec 90]	2
Incandescence in Liquids [N. Ye. Kask, Ye. G. Leksina, et al.; <i>TEPLOFIZIKA VYSOKIKH TEMPERATUR</i> Vol 28 No 6, Nov-Dec 90]	2
Energy Dissipation in Stress Waves During Phase Transformations [A. V. Zhukov; <i>FIZIKA GORENIYA I VZRYVA</i> Vol 26 No 6, Nov-Dec 90]	2
Damping of Shock Waves in Foam Upon Explosion of Condensed Explosive Substance [B. I. Palamarchuk, A. T. Malakhov; <i>FIZIKA GORENIYA I VZRYVA</i> Vol 26 No 6, Nov-Dec 90]	3
Experimental Study of Flow in Transmitted and Reflected Transient Air Shock Wave Following Explosion of Charge [B. L. Glushak, E. E. Lin, et al.; <i>FIZIKA GORENIYA I VZRYVA</i> Vol 26 No 6, Nov-Dec 90]	3
Interferometry of Shock Waves in Gas-Discharge Plasma [A. I. Klimov, G. I. Mishin; <i>PISMA V ZHURNAL TEKHNIЧЕСКОY FIZIKI</i> Vol 16 No 24, 26 Dec 90]	4
Detection of Secondary Sound Generation in Liquid During Bulk Boiling Under Laser Treatment [O. A. Bukin, V. I. Ilichev, et al.; <i>PISMA V ZHURNAL EKSPERIMENTALNOY I</i> <i>TEORETICHESKOY FIZIKI</i> Vol 52 No 12, 25 Dec 90]	4

CRYSTALS, LASER GLASSES, SEMICONDUCTORS

Possibility of Attaining Stimulated Radiation Emission in Semiconductors by Means of Impact-Ionization Waves [I. V. Grekhov, V. M. Yefanov; <i>PISMA V ZHURNAL TEKHNIЧЕСКОY FIZIKI</i> Vol 16 No 17, 12 Sep 90] ...	5
New Method of Recording Vapors of Nonmesogenic Substances Using Nematic Liquid Crystals [D. F. Aliyev, I. I. Gasanov; <i>PISMA V ZHURNAL TEKHNIЧЕСКОY FIZIKI</i> Vol 16 No 23, 12 Dec 90]	5
Addition of Antimony to Silicon During Low-Temperature Molecular-Beam Epitaxy [B. Z. Kanter, A. I. Nikiforov, et al.; <i>PISMA V ZHURNAL TEKHNIЧЕСКОY FIZIKI</i> Vol 16 No 24, 26 Dec 90]	5
Thermally Stimulated PN-Junctions [I. K. Kamilov, M. M. Gadzhaliyev; <i>PISMA V ZHURNAL EKSPERIMENTALNOY I TEORETICHESKOY</i> <i>FIZIKI</i> Vol 52 No 12, Dec 90]	6

LASERS

Evolution of Electrophysical and Structural Properties of GaAs Layers Under Pulsed Laser Radiation [B. G. Gribov, G. M. Gusakov, et al.; <i>DOKLADY AKADEMII NAUK SSSR</i> Vol 314 No 3, Sep 90]	7
Supercompression of Pulse in Laser With Nonlinear Cavity [A. G. Bulushev, Ye. M. Dianov, et al.; <i>PISMA V ZHURNAL TEKHNIЧЕСКОY FIZIKI</i> Vol 16 No 23, 12 Dec 90]	7
Formation of Breakdown Channel in ZnSe by Continuous-Wave CO ₂ -Laser Radiation [S. Kh. Kushnir, B. R. Kiyak, et al.; <i>UKRAINSKIY FIZICHESKIY ZHURNAL</i> Vol 35 No 12, Dec 90] ..	8
Feasibility of Laser Emission in Al/Mg System Optically Pumped by Liner Radiation [V. V. Loskutov, V. I. Oreshkin; <i>PISMA V ZHURNAL EKSPERIMENTALNOY I TEORETICHESKOY</i> <i>FIZIKI</i> Vol 52 No 12, 25 Dec 90]	8

NUCLEAR PHYSICS

Experiments by Activation Method in Search of Neutron Nuclei [D. V. Aleksandrov, Ye. Yu. Nikolskiy, et al.; YADERNAYA FIZIKA Vol 52 No 4(10), Oct 90]	9
Effect of Scattering on Two-Particle Correlations of Identical Pions [M. I. Podgoretskiy; YADERNAYA FIZIKA Vol 52 No 4(10), Oct 90]	9
Instability of Nucleonic Dirac Sea in Relativistic Collisions [I. N. Mishustin; YADERNAYA FIZIKA Vol 52 No 4(10), Oct 90]	9
Expansion of Effective Radius for dt-Scattering and dt → nα Fusion [B. M. Karnakov, V. D. Mur, et al.; YADERNAYA FIZIKA Vol 52 No 6(12), Dec 90]	10
Measurement of Spectrum of Electron Antineutrinos From Nuclear Reactor [Yu. V. Klimov, V. I. Kopeykin, et al.; YADERNAYA FIZIKA Vol 52 No 6(12), Dec 90]	10
Possibility of Measuring Energy of Tritium β-Decay Edge by X-Ray Spectroscopy [A. Ainsaar; IZVESTIYA AKADEMII NAUK ESTONII: FIZIKA, MATEMATIKA Vol 39 No 4, Oct-Dec 90]	11
Measurement of Ultrashort Dephasing Time in Extrinsic Glasses With Noncoherent Laser Pulses [R. Kaarli, M. Ratsep; IZVESTIYA AKADEMII NAUK ESTONII: FIZIKA, MATEMATIKA Vol 39 No 4, Oct-Dec 90]	11
Structural Electron Microscopy of 08Mn2Si Steel Wire Drawn With Electrical Stimulation [V. Ye. Gromov, Yu. F. Ivanov, et al.; IZVESTIYA VYSSHIKH UCHEBNYKH ZAVEDENIY: FIZIKA Vol 33 No 12, Dec 90]	12
Anomalous Temperature Dependence of Lower Critical Magnetic Field for High-T _c Superconductor Ceramic [M. A. Baranov, V. S. Gorbachev, et al.; PISMA V ZHURNAL EKSPERIMENTALNOY I TEORETICHESKOY FIZIKI Vol 53 No 2, 25 Jan 91]	12
Correlated Acoustic and Neutron Emission From Deuterium-Impregnated Palladium Target [P. I. Golubnichiy, V. V. Kuzminov, et al.; PISMA V ZHURNAL EKSPERIMENTALNOY I TEORETICHESKOY FIZIKI Vol 53 No 2, 25 Jan 91]	13

OPTICS, SPECTROSCOPY

Measurement of Optical Rotation Angle With Subnanosecond Time Resolution [M. V. Arkhipov, S. V. Pavlov, et al.; IZVESTIYA VYSSHIKH UCHEBNYKH ZAVEDENIY: FIZIKA Vol 33 No 9, Sep 90]	14
Channeling and Collimation of and Radiation Emission by Relativistic Electrons in Nonuniform Superhigh-Intensity Light Fields [A. V. Andreyev, S. A. Akhmanov; PISMA V ZHURNAL EKSPERIMENTALNOY I TEORETICHESKOY FIZIKI Vol 53 No 1, Jan 91]	14
Anomalies in Spectral-Angular Distribution of γ-Radiation Emission by Ultrarelativistic Electrons in Thick Crystals [A. P. Antipenko, S. V. Blazhevich, et al.; PISMA V ZHURNAL EKSPERIMENTALNOY I TEORETICHESKOY FIZIKI Vol 53 No 1, Jan 91]	14
Possibility of Producing New Integrated-Optics Polarizers and Waveguide- Mode Transformers [A. A. Voyevodin, V. P. Gladkiy, et al.; PISMA V ZHURNAL TEKHNICHESKOY FIZIKI Vol 16 No 24, 26 Dec 90]	15
Quantum Fluctuations Annihilate Optical Soliton [A. V. Belinskiy; PISMA V ZHURNAL EKSPERIMENTALNOY I TEORETICHESKOY FIZIKI Vol 53 No 2, 25 Jan 91]	15
Generating High-Intensity Radiation Fluxes and Megabar Pressures in Liner Systems [V. A. Gasilov, S. V. Zakharov, et al.; PISMA V ZHURNAL EKSPERIMENTALNOY I TEORETICHESKOY FIZIKI Vol 53 No 2, 25 Jan 91]	16

PLASMA PHYSICS

Outlook for Practical Use of Thermonuclear Fusion With Magnetic Plasma Confinement [I. N. Golovin; FIZIKA PLAZMY Vol 16 No 12, Dec 90]	17
Possibility of Cosmic Rays Being Generated in Plasma Pinches [V. P. Vlasov, S. K. Zhdanov, et al.; FIZIKA PLAZMY Vol 16 No 12, Dec 90]	17
Microwave Breakdown of Atmospheric Air in Strong Light Fields [I. V. Sokolov; FIZIKA PLAZMY Vol 16 No 12, Dec 90]	17
Transport of Relativistic 100 kJ Microsecond Electron Beam Through Gas and Plasma in Strong Magnetic Field [B. A. Knyazev, P. I. Melnikov, et al.; FIZIKA PLAZMY Vol 16 No 12, Dec 90]	18
Conditions for Effective Energy Radiation Into Plasma [N. A. Zhizhnyak, N. M. Yatsenko; UKRAINSKIY FIZICHESKIY ZHURNAL Vol 35 No 12, Dec 90]	18
Plasma Channel Formation in Nitrogen During Electron Beam Injection [V. P. Grigoryev, A. G. Potashev; IZVESTIYA VYSSHIKH UCHEBNYKH ZAVEDENIY: FIZIKA Vol 33 No 12, Dec 90]	19

Microwave Discharges in Stratosphere and Their Effect on State of Ozone Layer [G. A. Askaryan, G. M. Batanov, et al.; <i>FIZIKA PLAZMY</i> Vol 17 No 1, Jan 91]	19
Theory of Microwave Discharge in Low-Pressure Gas [Yu. R. Alanakyan; <i>PISMA V ZHURNAL EKSPERIMENTALNOY I TEORETICHESKOY FIZIKI</i> Vol 17 No 1, Jan 91]	20

SUPERCONDUCTIVITY

Vortex Entrainment by Magnetostatic Wave in Composite Ferrite and High- T_c Superconductor Structure [N. I. Polzikova, A. O. Rayevskiy; <i>PISMA V ZHURNAL TEKHNIЧЕСКОY FIZIKI</i> Vol 16 No 17, 12 Sep 90]	21
Thermodynamics of Metal-to-Superconductor Transition [N. N. Sirota; <i>DOKLADY AKADEMII NAUK SSSR</i> Vol 314 No 3, Sep 90]	21
Synthesis and Physical Properties of Tl-Ca-Ba-Cu-O High- T_c Superconductors [G. A. Petrakovskiy, V. Ye. Volkov, et al.; <i>IZVESTIYA VYSSHIKH UCHEBNYKH ZAVEDENIY: FIZIKA</i> Vol 33 No 9, Sep 90]	21
Quantum Interference in Tl-Ca-Ba-Cu-O High- T_c Superconductor Ceramics [D. A. Velikanov, G. S. Patrin, et al.; <i>IZVESTIYA VYSSHIKH UCHEBNYKH ZAVEDENIY: FIZIKA</i> Vol 33 No 9, Sep 90]	22
Damon-Eschbach Waves in Ferromagnetic Film With Superconductor Coating [Yu. I. Bespyatykh, A. D. Simonov, et al.; <i>PISMA V ZHURNAL TEKHNIЧЕСКОY FIZIKI</i> Vol 16 No 23, 12 Dec 90]	22
Phonon Mechanism of Superconductivity in Strongly Correlated Systems [A. O. Anokhin, V. Yu. Irkhin, et al.; <i>PISMA V ZHURNAL EKSPERIMENTALNOY I TEORETICHESKOY FIZIKI</i> Vol 53 No 1, 10 Jan 91]	23

THERMODYNAMICS

Effect of Temperature Gradient on Thermodynamic and Correlation Characteristics of Nonhomogeneous Substance Near Critical Point [A. D. Alekhin, L. A. Bulavin; <i>UKRAINSKIY FIZICHESKIY ZHURNAL</i> Vol 35 No 12, Dec 90]	24
---	----

THEORETICAL PHYSICS

Fluctuation Spectrum in Exactly Solvable Model With Dissipation: New Model of Flicker Noise [O. Yu. Dinariyev; <i>IZVESTIYA VYSSHIKH UCHEBNYKH ZAVEDENIY: FIZIKA</i> Vol 33 No 18, Oct 90]	25
Mechanism of P- and CP-Invariance Violation in Nonassociative Field Theory [D. F. Kurdgelaidze, G. A. Begeluri; <i>IZVESTIYA VYSSHIKH UCHEBNYKH ZAVEDENIY: FIZIKA</i> Vol 33 No 10, Oct 90]	25

Observation of Standing Surface Acoustic Waves in Crystals by Methods of X-Ray Topography

917J0024A Leningrad PISMA V ZHURNAL
TEKHNICHESKOY FIZIKI in Russian Vol 16 No 17,
12 Sep 90 pp 5-9

[Article by O. P. Aleshko-Ozhevskiy, A. S. Pogosyan, V. V. Lider, and V. I. Pyshnyak, Institute of Crystallography imeni A. V. Shubnikov, USSR Academy of Sciences, Moscow]

[Abstract] Since effective operation of SAW devices requires retention of the straight phase front during its passage through a crystal between radiator and receiver, it becomes necessary to study its interaction with surface defects. This has been done by the stroboscopic method, which requires synchrotron radiation suitably varying in time. This can also be done using methods of x-ray diffraction topography, with standing surface acoustic waves generated in the crystal by interaction of two arrays of traveling waves which have the same frequency and propagate in opposite directions. Two such methods were tried on two acoustoelectronic delay lines, namely on Y-cuts of a quartz crystal whose natural frequency was 30.5 MHz natural frequency and a LiNbO_3 crystal whose natural frequency was 46 MHz. For both methods a 1.5BSV-29 x-ray tube with a CuK_α -radiation source was used. First, the one-crystal reflection method with scanning of both the crystal surface and the photographic plate was tried. Then, the two-crystal method was used with the x-ray beam collimated and widened to 2 mm during passage through a Ge-(211) monochromator with a set of (311) planes asymmetrically reflecting the beam prior to its incidence on the crystal surface. Traveling surface acoustic waves were generated by interdigital transducers converting sinusoidal electric signals with an amplitude of about 5 V from a G4-143 oscillator, radiators and receivers being simultaneously excited by signals from the same oscillator so that counterpropagating waves of the same frequency would interact on the crystal surface and thus produce standing waves. Both amplitude and frequency of such standing waves would remain constant in the absence of surface defects. Their distribution pattern around a surface defect would become distorted, however, not exactly matching the instantaneous distribution of the traveling waves and depicting changes in their phase fronts. The contrast pattern of such standing waves indicates the local amplitudes as well as the phase shifts of the traveling waves which, owing to the use of short-wave radiation, can thus be measured more precisely than by laser interferometry. In the case of surface acoustic waves with frequencies above 100 MHz, recording on RMA photoresists will ensure a submicrometer resolution not attainable on photographic plates. Since the sensitivity of these photoresists is much lower than that of photographic plates, however, it would in this case be preferable to use the faster two-crystal method. Figures 3; references 3.

Processing and Interpretation of Experimental Data on Microwave Interferometry of Shock Waves in Weakly Ionized Plasma

917J0036A Moscow TEPILOFIZIKA VYSOKIKH
TEMPERATUR in Russian Vol 28 No 6, Nov-Dec 90
pp 1041-1047

[Article by A. P. Yershov, S. V. Klishin, S. V. Kuzovnikov, S. Ye. Ponomareva, and Yu. P. Pytyev, Moscow State University imeni M. V. Lomonosov]

UDC 533.9.01

[Abstract] Experimental data on diagnostic microwave interferometry of shock waves in a high-frequency discharge plasma are interpreted on the basis of a theoretical analysis, processing the data by the reduction method having improved the spatial resolution of the interferometer. The experiment was performed in a shock tube with a 45 mm circular diaphragm and a quartz discharge tube having the same diameter, this discharge tube having been calibrated and filled with air or argon under pressures of 10 - 1000 Pa before a transverse 40 MHz discharge was triggered inside it between two 20 cm long external electrodes. The electronic component of ensuing shock waves was measured with a classical Golant interferometer (V. Ye. Golant, 1968) operating at the $\lambda = 8$ mm wavelength and having antennas made of a dielectric material such as polystyrene, their approximately 20:1 length-to-diameter ratio ensuring a nearly minimum light beam divergence. Attenuation of the probing wave was minimal, inasmuch as its frequency was much higher than the discharge frequency. The discharge generated a cylindrical plasma column with a diameter larger than $3\lambda = 24$ mm and thus sufficiently large for using the model of a plane layer for data analysis in the approximation of geometrical optics. The plasma had an electron concentration within the $n_e = 10^{10} - 10^{11} \text{ cm}^{-3}$ range, much lower than one tenth the critical one, and was in the absence of a shock wave homogeneous in a plane normal to the probing light beam. It becomes nonhomogeneous in the presence of a shock wave, and herein lies the principle of structural shock wave analysis based on the relation between the phase shift of the interferometer signal and the electron concentration in the charged component of the shock wave. The problem is readily reduced to a one-dimensional one, the phase shift being equal to the integral of n_e (function of the $x - vt$ coordinate) multiplied by the instrument correction (function of the x -coordinate), with a further correction for an additive noise component (function of time) in the interferometer signal. Analysis of the electronic shock wave component based on the given scheme of measurement, taking into account the cooling of electrons and the attendant energy losses caused by their elastic and inelastic collisions with vibrationally excited neutral gas particles, indicates that a shock wave in the plasma of atomic and molecular gases is preceded by a rarefaction wave. Figures 3; references 15.

Peculiarities and Time Characteristics of Radiation Emission by Plasma Shock-Injected Into Air

917J0036B Moscow *TEPLOFIZIKA VYSOKIKH TEMPERATUR in Russian* Vol 28 No 6, Nov-Dec 90 pp 1086-1092

[Article by A. F. Aleksandrov, K. Sh. Isayev, I. B. Timofeyev, V. A. Chernikov, and U. Yusupaliyev, Moscow State University imeni M. V. Lomonosov]

UDC 537.523

[Abstract] An experimental study of radiation emission by a plasma shock-injected into air was made in a "Foton" apparatus with two pulsed plasmotrons. One plasmatron had a large discharge chamber (100 cm³) across a 144 - 288 μ F capacitor bank charged to 5 - 40 kV and one plasmatron had a small discharge chamber (3 cm³) across a 40 μ F capacitor bank charged to 5 - 25 kV. The discharge current was a damped sinusoidal one with a 67 - 79 μ s quasi-period in each chamber, its maximum amplitude being 450 kA in the large one and 35 kA in the small one. After evacuation, each discharge chamber was filled either with xenon to initial pressures of 0.01 - 0.4 MPa or with air to an initial pressure of 0.07 MPa. The current-voltage characteristics of discharge were measured with a noninductive voltage divider and a Rogowski loop. Spectral and time characteristics of radiation emission by the plasma jet flowing into atmospheric air and by evolving plasma formations were measured with two spectrographs (ISP-30, STE-1) using various photomultipliers and with two photoelectric calorimeters (FEK-09, FEK-15). A special mechano-electronic shutter in front of the spectrograph improved both spatial and time resolutions. The data reveal long-lived glow of plasma formations, of particular interest being the spherical ones. Their emission and absorption spectra were found to contain lines attributable to elements in the chemical composition of the metal electrodes and the dielectric chamber walls, such formations evidently containing neutral atoms of those elements and not only molecules of their oxides but also C₂ and CN molecules. Such a spherical plasma formation as well as the toroidal plasma vortex in the remaining "mushroom hat" do not seem to significantly influence the total energy emitted by the plasma. Figures 3; references 14.

Incandescence in Liquids

917J0036C Moscow *TEPLOFIZIKA VYSOKIKH TEMPERATUR in Russian* Vol 28 No 6, Nov-Dec 90 pp 1048-1055

[Article by N. Ye. Kask, Ye. G. Leksina, G. M. Fedorov, and M. T. Yaborov, Institute of Nuclear Physics and Moscow State University imeni M. V. Lomonosov]

UDC 535.211.22:533.9.082.3

[Abstract] An experimental study of laser action on liquids resulting in initiation and propagation of optical discharge was made, quasi-continuous 1.06 μ m radiation

with 20 percent intensity modulation from a neodymium laser being focused by a lens into a cylindrical cavity with liquid in pulses of 10 ms duration. Cylindrical holes 3 - 5 mm long and 2 - 3 cm in diameter were drilled into monoblocs of quartz glass or silicate glass, to ensure efficient heating with minimum energy losses due to hydrodynamic effects, and covered by a quartz glass plate with a coat of lampblack for optical contact. Tests were performed with water (addition of blue vitriol raising the absorption coefficient to approximately 1 cm⁻¹) ethanol, glycerin, acetone, benzene, toluene, CCl₄, and several water-base electrolytes (HCl, NaCl, NaOH, Na₂SO₄, KBr). Boiling was prevented by raising the pressure above critical without exceeding the mechanical strength of the monobloc. Images of the interaction region were projected onto the cathodes of two photomultipliers (FEU-30, FEU-62). The effective brightness temperature at 0.47 μ m and 0.62 μ m wavelengths was measured with an SI8-200U flash-lamp as reference-brightness source. Also the color temperature was measured. Spectral bands were extracted by means of interference filters. The threshold temperature for initiation of optical discharge was determined by immersion of a tungsten foil in the liquid, this foil absorbing the laser radiation and generating heat. A control test without such a foil revealed that presence of such a foil did not significantly influence the decomposition of liquid molecules and thus the step change of the absorption coefficient. The results of this experiment are compared with available data on the thermodynamics of laser-induced decomposition reactions, typically decomposition of acetone and water, some characteristics of optical discharge in this experiment indicating its wide deviation from an ideal one. Figures 5; tables 1; references 26.

Energy Dissipation in Stress Waves During Phase Transformations

917J0049A Novosibirsk *FIZIKA GORENIYA I VZRYVA in Russian* Vol 26 No 6, Nov-Dec 90 pp 124-127

[Article by A. V. Zhukov, Tomsk]

UDC 620.186:539.42

[Abstract] Conversion of mechanical energy into heat at polymorphic phase transformations in iron ($\alpha \rightarrow \epsilon$, $\epsilon \rightarrow \alpha$) and in titanium ($\alpha \rightarrow \omega$, $\omega \rightarrow \alpha$) is quantitatively analyzed by numerical simulation of a model process, namely impact of a plate on a rigid wall. The mathematical model contains the equations of motion for an elastoplastic body undergoing phase transformations and the equations of state for the metallic phases. Parameters in these equations include the 298 K reference temperature and the thermodynamic potential Φ which determines the interphase boundary. This system of equations is supplemented with a set of equations of phase transformation kinetics, for the rates of change of concentrations, in a system of i phases during martensite transformation. The numerical analysis is based on an

impact velocity of 600 m/s and following values of phase transformation parameters: temperature and pressure (335 K and 11.2 GPa for $\alpha \rightarrow \epsilon$, 304 K and 2.04 GPa for $\alpha \rightarrow \omega$), change of specific volume (-6.34 and -3.53 cm^3/kg), change of entropy (0.023 and -0.034 kJ/kg.K), change of enthalpy (78.7 and -3.0 kJ/kg), and derivative of thermodynamic potential with respect to pressure $d\Delta\Phi/dp$ (-6.3 kJ/kg.GPa for $\alpha \rightarrow \epsilon$, -3.4 kJ/kg.GPa for $\alpha \rightarrow \omega$). Calculations have yielded pressure and temperature profiles at the center of an iron or titanium plate as well as pressure and temperature transients at some point of such a plate. The profiles reveal a hysteresis of phase transformation in a stress wave, with supercompression under a decreasing load and overextension under a decreasing load. The amount of energy dissipated according to this model is higher than actually dissipated in a three-dimensional system under an omnilateral load, but the order of magnitude is the same and these estimates are quite adequate. Figures 2; tables 2; references 4.

Damping of Shock Waves in Foam Upon Explosion of Condensed Explosive Substance

917J0049B Novosibirsk FIZIKA GORENIYA I
VZRYVA in Russian Vol 26 No 6, Nov-Dec 90
pp 135-143

[Article by B. I. Palamarchuk and A. T. Malakhov, Kiev]

UDC 533.529+533.593

[Abstract] Explosion of a condensed explosive in foam, a two-phase medium, is analyzed for the effectiveness of such a shield in damping emitted shock waves. Considering that both gaseous and condensed phases flow at the same velocity when the characteristic time of flow development following the explosion is much longer than the characteristic time of phase velocity-equilibrium stabilization, the equation of state for the foam as a vapor-liquid mixture at thermal equilibrium is formulated by first ignoring evaporation of the condensed phase under thermodynamic equilibrium and then including its evaporation but assuming the vapor to be an ideal gas. The thermodynamic parameters for these equations of state have been determined on the basis of Dalton's law and the Clausius-Clapeyron equation. The equation of state for the detonation products is formulated using the pressure on the detonation wavefront at the Chapman-Jouguet point. These equations are supplemented by two dimensionless equations of motion for foam and for detonation products respectively: acceleration $\delta U/\theta = -v(r/\lambda)^{\gamma} \delta p/\delta \lambda$ (Euler coordinate $r = R/\alpha$, Lagrange coordinate $\lambda = \Lambda/\alpha$, $\delta r/\delta \theta = u$, $\delta \lambda/\delta \theta = -p\delta v/\delta g v$, p - pressure, specific volume $v = v_0(r/\lambda)^{\gamma} \delta r/\delta \lambda$, $v = 1, 2, 3$ for plane, cylindrical, spherical symmetry respectively). An analytical solution of the complete system of equations has yielded the relevant relations between macroscopic shock wave parameters. Its numerical solution on a Standard System 1040 computer for water-air foam and spherical symmetry, under specific conditions (ambient

temperature 293 K, atmospheric pressure 101,325 Pa, pressure at Chapman-Jouguet point 19.32 MPa, adiabatic exponent $\gamma = 1.4k$), has yielded values of both pressure and internal energy at various points on successive shock fronts at instants of time at which the front of the leading shock wave had reached distances from the explosion center equal to 10, 20, 30 radii of the spherical charge slug. The results indicate that accounting for evaporation of the condensed phase has not significantly altered the overall pattern. There are appreciable differences, however, between the results of these calculations and known experimental data. The discrepancy is largely attributable to nonadiabatic expansion of detonation products, associated with two factors influencing the behavior of the boundary between foam and detonation products: favorable conditions for that boundary developing a Rayleigh-Taylor instability during the initial expansion of detonation products and inertia of liquid foam drops causing them, during their initial growth, to cross that boundary into the region of detonation products. Figures 3; references 21.

Experimental Study of Flow in Transmitted and Reflected Transient Air Shock Wave Following Explosion of Charge

917J0049C Novosibirsk FIZIKA GORENIYA I
VZRYVA in Russian Vol 26 No 6, Nov-Dec 90
pp 143-145

[Article by B. L. Glushak, E. E. Lin, and S. A. Novikov, Moscow]

UDC 533.6.011.72

[Abstract] Experiments with air shock waves generated by explosion of a charge were performed for a study of air flow in such waves. Air flow in a shock wave reflected by a rigid barrier was studied in three shock tubes 0.51 m, 0.76 m, and 1 m long respectively, with the charge 0.5 m away from the closed end of a tube. Passage of a shock wave reflected by the back wall of such a tube was recorded in the form of $x(\text{distance}) - t(\text{time})$ diagrams for the shock front, with the aid of piezoelectric pressure transducers along the lateral tube wall. It was also recorded by an oscillograph, interaction of the reflected shock wave and the boundary layer in a tube having been taken into account in analysis of the oscillograms. Air flow in a strong transmitted shock wave was studied in a steel tube 0.6 m in diameter, with a charge also 0.6 m in diameter inside a thin shell placed at the entrance to the tube and a 0.1 m thick layer of explosive triggered from outside at many points so as to cause explosion with an energy density of approximately 0.9 GJ/m^2 . Passage of a shock wave through this tube was recorded by pressure transducers of the electric-contact type spaced 0.5 m apart along the lateral tube wall. The experimental data are compared and found to agree closely with a numerical solution to the equations of gas dynamics for one-dimensional air flow and the cubic equation of state for

detonation products, air being regarded as an ideal gas. Figures 1; tables 1; references 7.

Interferometry of Shock Waves in Gas-Discharge Plasma

917J0058B Leningrad PISMA V ZHURNAL
TEKHNICHESKOY FIZIKI in Russian Vol 16 No 24,
26 Dec 90 pp 89-94

[Article by A. I. Klimov and G. I. Mishin, Institute of Engineering Physics imeni A. F. Ioffe, USSR Academy of Sciences, Leningrad]

[Abstract] An experimental study of shock waves in a cold air plasma was made concerning the transient characteristics of density profiles behind the shock front. Nonstationary transverse glow discharge with a current density up to 30 mA/cm^2 under a pressure up to 12 torr in a vertical shock tube with a 100 mm square cross-section and a single diaphragm was produced by a bank of 2 - 100 μF capacitors with a 51 k Ω ballast resistor each, a TGI-500/16 thyatron being used as switch. The cathode, at the lower end of the tube, was segmented into three rows of seven disk electrodes in each. The solid anode above, 100 mm wide and 170 mm long was grounded. The tube, made of caprolon, had several 200 mm long and 100 mm high windows made of optical glass in its lateral walls. The air density and temperature distributions were measured with a Michelson interferometer, a high sensitivity having been attained by making the light beam pass through an optical inhomogeneity twice. Fast pressure changes were recorded with a piezoelectric transducer. As a continuous light source was used an LGN-215 single-mode He-Ne laser ($0.63 \mu\text{m}$ wavelength), with a single beam generating the time base and an FEU-86 photomultiplier recording the shifts of interference fringes. A pulsed laser ($0.53 \mu\text{m}$ wavelength) with a passive shutter producing pulses of 20 - 40 ns duration was used for shooting individual frames, the interferograms then being photographed on A-2 film in a camera with a mechanical shutter. The discharge current density was varied over the 20-30 mA/cm^2 range. The air pressure P was varied from below 3 torr to 12 torr, normal discharge within the $P = 3 - 12$ torr pressure range being characterized by $E/P = 6 - 8 \text{ V/(cm.torr)}$ and abnormal discharge under pressure lower than 3 torr being characterized by $E/P = 20 - 30 \text{ V/(cm.torr)}$ (E - supply voltage minus cathode drop). Also the duration of glow discharge was varied from 30 μs to 400 μs , the current increasing correspondingly to a constant magnitude in glow discharge sustained longer than 100 μs and the velocity of a shock wave decreasing from 160 m/s to 125 m/s as the voltage dropped from breakdown level to ignition level. The plasma remained cold, its temperature remaining within the 230 - 370 K range except within a not wider than 10 mm layer near-cathode layer where it could become as high as to 700 - 1100 K.

Analysis of the interferograms and readings of the pressure transducer indicate that a shock wave propagating through the plasma of a glow discharge had split into two, a forerunner and trailer with both fronts about 10 times wider than in air without glow discharge. Upon entry into a hot near-cathode layer, a shock wave was found to decay either into a very elongated compression wave with a smooth density profile or a weak compression shock with a slanted density profile. In an experiment with high current density $j \geq 30 \text{ mA/cm}^2$ and glow discharge duration $t \approx 400 \text{ ns}$ in an air plasma under pressure $P \geq 3$ torr, $E/P = 20 - 40 \text{ V/(cm.torr)}$, the forerunner was preceded by a leader with a front which propagated much faster, about 200 m/s faster, and left a lower air density behind. Figures 3; references 3.

Detection of Secondary Sound Generation in Liquid During Bulk Boiling Under Laser Treatment

917J0060A Moscow PISMA V ZHURNAL
EKSPERIMENTALNOY I TEORETICHESKOY
FIZIKI in Russian Vol 52 No 12, 25 Dec 90
pp 1261-1263

[Article by O. A. Bukin, V. I. Ilichev, and V. D. Kiselev, Pacific Oceanographic Institute, Far Eastern Department, USSR Academy of Sciences]

[Abstract] An experiment was performed concerning generation of sound in a liquid brought to bulk boiling by high-intensity optical radiation. It was performed with a CO_2 -laser emitting $10.6 \mu\text{m}$ radiation in pulses of 100 J energy and 9 μs total duration. This radiation was focused by a lens onto the surface of sea water so as to form a spot 3 cm in diameter. Bubble boiling under that spot was ensured by a radiation power density exceeding 2.5 J/cm^2 . Acoustic signals were recorded with a calibrated hydrophone covering the frequency range up to 300 kHz, their waveform being correctly duplicated by its electric output signals. A computer-aided analysis of that waveform revealed not only a main sound pulse representing the response to incidence of a vapor-droplet jet formed as a result of bulk boiling but also a trailing second pulse. The lag time was 20 μs , almost the same in all readings taken at various depths down to 100 m below the surface and at various angles to the vertical laser beam. The amplitude of this trailing pulse was consistently smaller than that of the main one, the 1:5 ratio remaining almost constant along the axis of the sinking laser beam. The trailing signal was also more directional than the main one. Therefore, inasmuch as the experiment had been set up so as to eliminate any reflection by the hydrophone and the possibility of diffraction by edges of its aperture giving rise to another acoustic signal, its source was most likely the laser spot on the water surface. The authors thank A. O. Maksimov for helpful discussions. Figures 2; references 4.

Possibility of Attaining Stimulated Radiation Emission in Semiconductors by Means of Impact-Ionization Waves

917J0024B Leningrad PISMA V ZHURNAL
TEKHNICHESKOY FIZIKI in Russian Vol 16 No 17,
12 Sep 90 pp 9-14

[Article by I. V. Grekhov and V. M. Yefanov, Institute of Engineering Physics imeni A. F. Ioffe, USSR Academy of Sciences, Leningrad]

[Abstract] An experiment with gallium arsenide was performed which demonstrated the possibility of attaining stimulated radiation emission in a semiconductor by means of an impact ionization wave, necessary for this sufficiently large volume of inverse electron-hole plasma having previously been produced only by either optical pumping or electron bombardment. It was attained in 0.09 mm wide and 0.25 mm long GaAs-diode structures on 0.25 mm thick n^+ substrates at room temperature, such a diode consisting of a 0.02 cm thick high-resistivity $n_0 - p_0$ base double layer and a 0.03 mm thick p^+ emitter layer. Such a diode was placed in the gap in a coaxial transmission line having a wave impedance of 50 Ω without matching impedance. The diode was excited with a voltage pulse, the voltage rising at a rate of 5×10^{13} V/s to an approximately 5.5 kV peak far above the avalanche breakdown level and then within about 100 ps falling to below 1 kV. Within that voltage fall time an impact ionization passed through $n_0 - p_0$ base region and produced an electron-hole plasma with concentration inversion. No surface or air breakdown occurred, despite absence of protective coatings on the lateral faces. The resulting current pulse of 1 ns duration induced emission of recombination radiation, which was passed through a focusing lens to the photocathode of an "Agat SF" image converter. The latter operated in the static mode without time sweep or in the dynamic mode with a time sweep of 250 ps/cm for photography and chronography of radiation emission at current densities up to 2000 kA/cm². The increase of the radiation intensity with increasing current density within the short pump pulse duration and without the latter having changed, an increase so steep as to require addition of up to five attenuating filters for photography, indicated that a transition to stimulated radiation emission had taken place at some threshold excitation level. The authors thank Yu. V. Zhilyayev for supplying the large GaAs structure from which the experimental diodes were then cut. Figures 2; references 9.

New Method of Recording Vapors of Nonmesogenic Substances Using Nematic Liquid Crystals

917J0053C Leningrad PISMA V ZHURNAL
TEKHNICHESKOY FIZIKI in Russian Vol 16 No 23,
12 Dec 90 pp 85-91

[Article by D. F. Aliyev and I. I. Gasanov, Baku State University]

[Abstract] An experimental study of nematic liquid crystals in vapors of organic substances was made, the results having revealed a relation between the change in the intensity of light transmitted by such a crystal and the dynamic viscosity of the vapor. The liquid crystal, nematic at room temperature, was a 1:1 mixture of n-methoxybenzylidene-para-n-butylaniline and n-ethoxybenzylidene-para-n-butylaniline. A film of this substance, 30 μ m thick with a 1 cm² free surface area and a planar orientation, was placed in a vessel of 15 dm³ capacity between two crossed polaroids. Vapor of an organic substance was admitted into the vessel, the temperature inside being maintained at 293 \pm 0.005°C and the air having been reduced to 680 mm Hg. Tests were performed with vapor of hexane, heptane, octane, acetone, and chloroform, also of benzene and toluene. The recorded effect of organic vapor on the light transmission by a nematic film crystal is interpreted on the basis of Malus' sine-squared law $I = I_0 \sin^2 \varphi \sin^2(\delta/2)$ (φ - angle between the director and the plane of polarization of incident light, $\delta = 2\pi d \Delta n / \lambda$, d - thickness of film, λ - wavelength of incident light, I_0 - intensity of incident light, Δn - difference between the refractive indices of film and vapor), angle φ being zero in the absence of vapor and increasing but Δn decreasing as vapor is admitted. The light transmission intensity was found to change gradually over some period of time up to 120 s, in different ways depending on the organic substance and on the concentration of its vapor. The data reveal two critical vapor concentrations, the lower one corresponding to a rotation of the director in the plane of the film and an attendant 5 percent change (in hexane vapor) of the light transmission intensity. Further increase of the vapor concentration results in an increase of the light transmission intensity and a shortening of the transmission peak duration, whether the director rotates clockwise or counterclockwise, up to the much higher upper critical one representing transition to an isotropic liquid attended by two consecutive transmission peaks. The lower first peak is associated with a fast rotation of the director from its equilibrium position and subsequent return to it. The higher second peak is associated with intense "boiling" and resembles EHD instability which precedes transition to an isotropic liquid. The mechanism of this process, under a pressure not far below atmospheric, evidently involves diffusion of vapor molecules in a direction approximately normal to the film and their subsequent absorption by it. A theoretical analysis based on Fick's law of diffusion kinetics yields a unique relation between changes in the light transmission by a nematic liquid crystal and the dynamic viscosity of the ambient organic vapor, the basis for a new method of determining the dynamic viscosity of an organic vapor at its lower critical concentration and thus responsible only for rotation of the director. Figures 2; tables 1; references 8.

Addition of Antimony to Silicon During Low-Temperature Molecular-Beam Epitaxy

917J0058A Leningrad PISMA V ZHURNAL
TEKHNICHESKOY FIZIKI in Russian Vol 16 No 24,
26 Dec 90 pp 1-6

[Article by B. Z. Kanter, A. I. Nikiforov, and S. I. Stenin, Institute of Semiconductor Physics, Siberian Department, USSR Academy of Sciences, Novosibirsk]

[Abstract] An experimental study of silicon doping with donor impurity during molecular-beam epitaxy at temperatures of 300-600°C was made, silicon vaporized by an electron-beam heater being deposited on Si(111) and Si(100) substrates for epitaxial growth at a constant rate of 0.3 nm/s and at the same time being doped with antimony from an evaporator crucible. The process at each temperature consisted of three stages, antimony being added at a rate $F[\text{Sb}] = 10^{12}$ atoms/(cm².s) in the second stage only. From measurements of the spreading resistance were determined the Sb concentration profiles $n(d)$ and the embedment factor $K = F[\text{Sb}]_e / F[\text{Sb}]_i$ ($F[\text{Sb}]_e$ - Sb atoms embedded in lattice of growing Si crystal, $F[\text{Sb}]_i$ - Sb atoms impinging on its surface). Both n_{max} and K were found to depend alike on the substrate temperature T_s but differently on the temperature of Si(111) and Si(100) substrates. Their dependence on the Si(111) substrate temperature is characterized by two ranges: in the high-temperature range both increasing exponentially ($K \rightarrow 1$) with an activation energy of 1.2 eV as T_s decreases to 500° and in the low-temperature range from 500°C down both increasing further very slightly. Transition to the low-temperature doping mode was accompanied by a change of the substrate surface structure from Si(111) - 7 x 7 to Si(111) - 1 x 1, according to a fast-electron diffraction analysis. Their dependence on the Si(100) substrate temperature is exponential throughout the entire range, here K increasing from 10^{-4} at 600°C to 10^{-1} at 300°C, with an activation energy of about 1 eV. Transition to the low-temperature doping mode on a Si(100) substrate evidently occurs within the 300 - 200°C temperature range, as indicated by a change of its surface structure from Si(100) - 2 x 1 to Si(100) - 1 x 1. The Sb-doping range in the low-temperature mode of molecular-beam epitaxy was determined on multilayer Si structures at a substrate temperature close to the threshold for each substrate orientation: 400°C and 300°C for a Si(111) and Si(100) substrates respectively. An almost linear relation was found to exist between the Sb flux $F[\text{Sb}]$ and the maximum charge carrier concentration, over the $F[\text{Sb}] = 10^9 - 10^{12}$ atoms/(cm².s) range. Figures 2; references 9.

Thermally Stimulated PN-Junctions

917J0060B Moscow PISMA V ZHURNAL
EKSPERIMENTALNOY I TEORETICHESKOY
FIZIKI in Russian Vol 52 No 12, 25 Dec 90
pp 1259-1260

[Article by I. K. Kamilov and M. M. Gadzhaliyev,
Institute of Physics, USSR Academy of Sciences, Dag-
estan branch]

[Abstract] A new method of producing p-n junctions is proposed which, unlike conventional alloying or diffusion, utilizes sign reversal of the Hall coefficient and the thermo-e.m.f. at the "inversion" temperature. Establishment of a temperature gradient along the semiconductor crystal so that one part of it is at a temperature above that point and one part of it is at a temperature below this point with the two part an n-type region and a p-type region respectively. Such a junction will be a dynamic one, athermally stimulated diode or rectifier, inasmuch as it will exist only while this temperature gradient is maintained. The validity of this principle was confirmed experimentally on silicon ($T_i \approx 420$ K) and germanium ($T_i \approx 370$ K) by measurement of the current-voltage characteristics in three tests. A temperature gradient was produced by means of a heater (temperature T_h) and a cooler (temperature T_c), with the semiconductor crystal in the first test all extrinsic part at a temperature below $T_i > T_h$, in the second test all intrinsic at a temperature above $T_i < T_c$, in the third test all at a temperature in the vicinity of T_i between T_c and T_h . Only in the third test was it feasible to produce a thermally stimulated p-n junction, and then to control the size of either region as well as the width of the junction by controlling the magnitude of the temperature gradient. For the p-Ge crystal, a 1 mm x 1 mm x 1.6 mm dumb-bell with an electrical resistivity of 50 Ω.cm, the temperature gradient was 1000°C/cm. The authors thank A. S. Borovik-Romanov for interest and helpful suggestions. Figures 1; references 2.

Evolution of Electrophysical and Structural Properties of GaAs Layers Under Pulsed Laser Radiation

917J0039A Moscow DOKLADY AKADEMII NAUK
SSSR in Russian Vol 314 No 3, Sep 90 pp 618-621

[Article by B. G. Gribov, corresponding member, USSR Academy of Sciences, G. M. Gusakov, T. N. Kodratova, Ye. N. Nagdayev, and A. V. Rodionov, Moscow Institute of Electronics Engineering]

UDC 621.315.592.2:546.681'19:621.375.826

[Abstract] An experimental study of pulsed laser treatment of epitaxial GaAs layers was made, its object being to determine the effect of pulsed laser radiation on their electrophysical and structural properties. For this purpose, 0.2 - 0.35 μm thick GaAs layers were deposited by gaseous-phase epitaxy on Cr-compensated substrates with a (100) orientation while being doped with Cd, Ge or with S. The initial concentration of free electrons in p-type and n-type covered the 1×10^{17} - 4×10^{18} range. The layers were refined by various methods and then treated with 530 nm radiation from a single-mode YAG-laser in pulses of 50 ns duration, stable within 5 percent and covering a spot with a 0.060 μm radius to the 0.6321_{max} intensity circle. They were thus treated either in air or under high pressure up to 200 atm in an Ar or O₂ cell. The density of incident radiation energy was varied from 0.4 J/cm² (above the surface melting level) to 0.8 J/cm² (below the breakdown level). The maximum depth of the melting zone was determined with the aid of a probing He-Ne laser beam. Conductivity and mobility profiles were by both Hall and vander Pauw methods, with layer-by-layer etching and use of a controllable oxidation layer. Concentration and parameters of deep levels were measured by the nonstatic capacitance-time method. The structure of 30 - 40 nm thick surface layers were examined by the method of high-energy electron diffraction in the reflection mode. The structure of 200 - 300 nm thick deeper layers was examined under a transmission electron microscope. The results indicate that laser radiation lowers the electrical conductivity of the surface layer, the thickness of this layer depending on the density of incident radiation energy but always remaining smaller than the maximum melting depth. Its thickness does not depend on the kind of impurity and neither on the method of preliminary surface refinement nor on the conditions of laser treatment. The results of measurements made in the course of subsequent layer-by-layer etching indicate that laser radiation had no effect on the charge carrier mobility, only on the concentration of free charge carriers which it lowered by at least one order of magnitude. The structure of 30 - 40 nm thick surface layers did, however, depend on the method of preliminary surface refinement as well as on the conditions of laser treatment as well as on the density of incident radiation energy. Dominance among deep levels in the n-type layers shifted from the E = 0.5 eV level with a $6 \times 10^{16}\text{cm}^{-3}$ concentration before to the E = 0.12 eV level with a $3 \times 10^{16}\text{cm}^{-3}$ concentration after

laser treatment. The thickness of the amorphous film on the surface decreased from its initial 5 - 10 nm thickness, depending on the method of surface refinement, to about 3 nm after laser treatment in air under atmospheric pressure but increased in the Ar cell up to a 30 nm maximum with either increasing radiation energy density or rising pressure. Inclusions of the 15 nm size fraction were in the 30 nm thick surface layer but no large structural defects in the bulk material were detected after laser treatment. Estimates based on these data yield an anomalously large diffusion coefficient, about 0.001 cm²/s, and a corresponding diffusion length of about 30 nm equal to the thickness of the surface oxide film produced by laser treatment in the O₂ cell. These estimates support the assertion based on experiments involving GaAs layers with about 30 nm deep As⁺-ion implantation layers, namely that laser treatment of such layers further degrades their electrophysical properties rather than restoring them, and thus provides an additional argument against the "vacancy" nature of their defects. Figures 4; references 13.

Supercompression of Pulse in Laser With Nonlinear Cavity

917J0053B Leningrad PISMA V ZHURNAL
TEKHNICHESKOY FIZIKI in Russian Vol 16 No 23,
12 Dec 90 pp 81-85

[Article by A. G. Bulushev, Ye. M. Dianov, and O. G. Okhotnikov]

[Abstract] Widening the spectrum of a laser pulse in a nonlinear cavity medium for subsequent compression of the pulse is considered, phase self-modulation being too weak and not significantly influencing the emission spectrum. As a more effective alternative is demonstrated, the possibility of a laser with such a cavity emitting radiation pulses with complete passive locking of modes close to the limits of its spectrum, a spectrum so much wider than the amplification range of the active medium as to make it appear supercompressed. The apparatus demonstrating this consists of an active medium in a cavity formed by a plane mirror and a nonlinear fiber-optic loop reflector with a nonreciprocal junction in the loop, the active medium having a uniformly broadened spectral line but its transparency window remaining much wider than its amplification range and both straight end segments of the fiber loop passing through an asymmetric common directional coupler. Propagation of radiation through the fiber is described by the nonlinear Schroedinger equation in a traveling system of coordinates. On this basis is theoretically demonstrated the evolution of a laser pulse from a random noise during passive mode locking by the nonlinear loop reflector. Numerical calculations have been made for specific values of the reflector parameters. A pulse at the entrance to the active medium has been obtained which represents a stable solution to that equation, its optical spectrum being marked by an amplitude-frequency characteristic $|A(\omega)|^2(\omega)$ symmetric relative to the $\omega = 0$ center frequency (corresponding to

maximum light amplification in the active medium within the "supercompressed" range) with a peak on each side of that center frequency beyond that amplification range and by a linear phase-frequency characteristic $\varphi(\omega)$ along which the phase decreases from maximum at the low-frequency limit to zero at the high-frequency limit. Figures 3; references 7.

Formation of Breakdown Channel in ZnSe by Continuous-Wave CO₂-Laser Radiation

917J0055A Kiev UKRAINSKIY FIZICHESKIY ZHURNAL in Russian Vol 35 No 12, Dec 90 pp 1796-1801

[Article by S. Kh. Kushnir, B. R. Kiyak, and M. G. Matsko, Institute of Physics, UkSSR Academy of Sciences, Kiev]

UDC 535.37:548.736

[Abstract] An experimental study of structural changes in polycrystalline ZnSe caused by continuous-wave CO₂-laser radiation was made, of particular concern being formation of a pass-through breakdown channel. Specimens of 2 mm thick ZnSe plates were placed on a ceramic stage and irradiated by an ILGN-704 industrial 30 W continuous-wave CO₂-laser with a power density of 0.1 and then 0.2 kW/cm² for up to 5 min, their temperature being monitored by a thermocouple. Structural changes resulting from this laser treatment were examined under a JSM-35 scanning electron microscope in three different modes: topography, composition, and cathodoluminescence. They were also examined by the x-ray diffraction method in a Weissenberg camera with a CuK α 1,2-radiation source and a Ni-filter. Absorption spectra were measured with an IFS-113 infrared spectrometer. Breakdown was found to occur in the form of both chemical and structural changes, a crater forming simultaneously on both front and back surfaces each underneath a ZnO film. An analysis of the results indicates that the temperature gradient in an irradiated ZnSe platelet is responsible for diffusion of intrinsic defects, which stimulates oxidation-reduction reactions and raises the oxygen content in the breakdown region, while a focusing thermal lens appears which distorts the wavefront of the infrared laser beam. As a ZnO subsurface film forms, the surface absorption coefficient for 10.6 μ m radiation increases appreciably so that heating of the surface becomes correspondingly more intense and buildup of the ZnO film is further enhanced. Such a positive feedback leads to thermal instability, formation of a ZnO film thus evidently being the principal cause of

intensified heating and subsequent evaporation of ZnSe under the laser spot till a pass-through hole is left. The optical effects of a thermal lens were found to be weaker in polycrystalline ZnSe than in ZnSe single crystals. Figures 5; references 4.

Feasibility of Laser Emission in Al/Mg System Optically Pumped by Liner Radiation

917J0060C Moscow PISMA V ZHURNAL EKSPERIMENTALNOY I TEORETICHESKOY FIZIKI in Russian Vol 52 No 12, 25 Dec 90 pp 1245-1248

[Article by V. V. Loskutov and V. I. Oreshkin, Institute of High-Current Electronics, Siberian Department, USSR Academy of Sciences]

[Abstract] An experimental laser is described with vapor of an originally solid target as active medium, the target having been both vaporized and pumped by a pulse of radiation emitted by a plasma liner upon its compression into a plasma column. The target is a layer of material forming a resonance-bound ion pair deposited on the inside surface of a cylindrical current return conductor, AlXI/MgIX having been selected as such an ion pair with radiation of 4.8338 nm wavelength corresponding to the resonance line of the $2s^2\ ^2S_{1/2} \rightarrow 3p^2\ ^1P_{1/2}^0$ transition in the lithium-like AlXI ion pumping the $2s^2\ ^1S_0 \rightarrow 2s4p\ ^1P_1^0$ transition in the beryllium-like MgIX ion (resonance line 4.834 nm). The radiation spectrum of the pumping source was determined according to the steady-state multilevel model of a multiply-charged dense homogeneous aluminum plasma layer, with given radius and height, electron temperature, and ion concentration. Radiation re-absorption was taken into account and the emission line was assumed to have a Voigt profile. Calculations were made according to the ATOM program, a typical pumping source being a plasma column 4 cm high with a 0.2 cm radius, an electron temperature of 200 eV, and an ion concentration of 3×10^{19} cm⁻³. Calculations for the active medium were based on the steady-state multilevel medium, including photoexcitation and photoionization by the pump as well as impact ionization. Photoionization from the ground state was found to be the principal ionization mechanism, photoexcitation of the MgIX ion being followed by its impact ionization. Parameters of the expanding active medium were calculated on the basis of the one-dimensional hydrodynamic model, including radiation transfer, electronic heat conduction, diffusion of the azimuthal magnetic field of the electric current flowing through the pinch-effect zone, Joule-effect heating by the return current, and the real rather than ideal thermodynamic properties of the active medium. Figures 3; references 6.

Experiments by Activation Method in Search of Neutron Nuclei

917J0044A Moscow YADERNAYA FIZIKA in Russian
Vol 52 No 4(10), Oct 90 pp 933-941

[Article by D. V. Aleksandrov, Ye. Yu. Nikolskiy, B. G. Novatskiy, and D. N. Stepanov, Institute of Atomic Energy imeni I. V. Kurchatov]

[Abstract] An experimental study was made in search of nuclear-stable multineutrons in ternary fission of ^{252}Cf using the activation method based on $^N\text{A}[\text{x-n}, (\text{x-k})\text{n}]^{N+k}\text{A}$ reactions, where ^{N+k}A denotes the β -active isotope with a measurable half-life of 10 - 100 h produced in such a reaction. The fission source, a specimen of ^{252}Cf weighing 19 μg , was deposited on a thick tantalum substrate so as to form on it an active spot about 10 mm in diameter and then covered with a 22 μm thick aluminum foil. Specimens of various isotopes in the form of cylinders 13.5 or 21 mm in diameter were placed in a container with a 22 μm thick aluminum window for bombardment, this container then having been hermetically sealed so as to prevent diffusion of active iodine radioisotopes, products of Cf fission, to the targets. The combined 44 μm thickness of both aluminum foils was adequate for shielding the targets against incidence of α -particles and fission fragments. The total distance from fission source to target was 3 mm. The total time of bombardment and measurement ranged from one to two half-life periods of the sought β -active isotope. Gamma rays were recorded by a low-background-noise γ -spectrometer with a 120 cm^3 large cylindrical detector made of pure germanium. A "well" had been drilled in this detector and the targets placed in it for spectrography in a 4π -geometry configuration. The detector was placed inside a hollow cylindrical NaI:Tl crystal as active shield and the latter in turn placed inside a 10 cm thick cylindrical lead vessel as passive shield, to prevent penetration of background γ -radiation and to suppress Compton scattering. Experiments performed with 6 - 200 mg specimens of the ^{26}Mg isotope did not reveal any significant activity of the sought ^{28}Mg isotope, expected product of the $^{26}\text{Mg}[\text{x-n}, (\text{x-2})\text{n}]$ reaction, evidently owing to a negligible direct two-neutron transfer. Neither did experiments with ^{19}F (using teflon), ^{25}Mg , ^{103}Rh , ^{110}Pd , ^{208}Pb isotopes reveal any significant activity of the sought isotope. The other known mechanism with a large cross-section, formation of a residual nucleus, has therefore been considered and the cross-sections for the various $\text{x-n}, (\text{x-k})\text{n}$ reactions calculated using the ALICE program (M. Blann, US ERDA report No COO-3494-29, 1976). Assuming then that nuclear-stable neutron nuclei do exist, the negative results are attributed to ineffective recording of MeV neutrons in that $\text{x-n}, (\text{x-k})\text{n}$ channel (the energy of fission neutrons here being most likely about 0.7 MeV). Slowdown of neutrons into the keV range and their attendant knock-out from the "beam" may be caused not only by their absorption in the moderator but also by elastic scattering ($\text{x-n}, \text{x-n}$), dissociation ($\text{x-n}, \text{x-n}$), and transfer of k neutrons $\text{x-n}, (\text{x-k})\text{n}$ in the moderator. An experiment was subsequently performed with an up to

32 MeV ^7Li ion beam in the Institute's cyclotron, in search of ^6n neutrons in the $^{14}\text{C}(^7\text{Li}, ^6\text{n})$ reaction. This exothermic reaction had been selected on account of its maximum cross-sections for multineutron transfers and most favorable energy level. Here activity of the ^{28}Mg isotope was recorded on the ^{14}C target, with use of a 1 mm thick tantalum filter, an activity evidently associated with the $^{26}\text{Mg}(\text{t}, \text{p})$ reaction involving high-energy tritons produced in the $^{14}\text{C}(^7\text{Li}, \text{t})$ reaction. This positive result confirms estimates of multineutron slowdown based on calculations by the Monte Carlo method, namely that the effectiveness of recording x-n neutrons can be increased by optimization of the experiment. The authors thank V. A. Denisov, V. M. Semochkin, and I. K. Shvetsov for producing the ^{252}Cf source, and M. V. Zhukov for discussing the results. Figures 5; tables 2; references 17.

Effect of Scattering on Two-Particle Correlations of Identical Pions

917J0044B Moscow YADERNAYA FIZIKA in Russian
Vol 52 No 4(10), Oct 90 pp 1123-1126

[Article by M. I. Podgoretskiy, Joint Institute of Nuclear Research, Dubna]

[Abstract] Pair correlations of identical pions generated inside a nuclear matter are analyzed, taking into account their generally inelastic scattering prior to their free propagation and starting with the simplest model of independent one-particle sources. Such a source located at some point r is at some time t assumed to emit a pion which has a momentum p and an energy ϵ . Considering that the amplitude of this emission process without subsequent scattering would be $A(p) = C e^{i(\epsilon p - t\epsilon)}$, the two-particle amplitude of emission of two identical pions (p', ϵ') and (p'', ϵ'') by two such sources (r_1, t_1), (r_2, t_2) is calculated accordingly. Next is considered emission of a pion (p_a, ϵ_a) at a point r_a and a time t_a with its subsequent elastic scattering by an immovable massive scatterer at a point r_b . While the law of energy conservation must be observed in this situation, the law of momentum conservation may be ignored. For comparison is then considered inelastic scattering of a pion at a point r_b where it meets particles of any kind which draw some of the initial energy ϵ_a from the incident pion. No difference in the pair correlations of identical pions is found in these two different events, which is further demonstrated with the aid of schematic scattering diagrams for each case. This does not, however, preclude the possibility of differences arising in more complicated situations. It is furthermore possible that scattering will give rise to interference correlations in pairs of nonidentical pions. The author thanks V. L. Lyuboshitz for important comments. Figures 2; references 4.

Instability of Nucleonic Dirac Sea in Relativistic Collisions

917J0044C Moscow YADERNAYA FIZIKA in Russian
Vol 52 No 4(10), Oct 90 pp 1135-1139

[Article by I. N. Mishustin, Institute of Atomic Energy imeni I. V. Kurchatov]

[Abstract] Nuclear matter containing a sea of nucleons subject to Dirac statistics and occupying a finite region of space sufficiently large for the nucleon density to be uniform except for its steep fall to zero across a thin surface layer is considered from the standpoint of relativistic fields and the underlying phenomenological Lagrangian, which describes nuclear matter, nuclear dynamics, and residual nuclei with inclusion of interacting nucleon and meson fields: at least one scalar field σ and one vector field ω^μ treated here as classical ones. The wave functions of these nucleons are approximated closely enough by plane waves and one-particle nucleon states are classified on the basis of their momentum in accordance with the steady-state Dirac equation, which describes simultaneously nucleons with energy $E_N = E^+(p)$ and antinucleons with energy $E_{N\text{-bar}} = -E^+(-p)$. Gradients of meson fields are ignored at zero temperature. It is shown that the mean vector potential increases linearly with increasing baryon density, while the effective mass of nucleons and antinucleons decreases with increasing baryon density and with rising temperature. In a baryon medium of sufficiently high density, moreover, the minimum energy of antinucleons can become lower than $-m_N$ so that the system becomes unstable with respect to spontaneous production of a nucleon-antinucleon pair at the boundary where the meson fields change appreciably. In a dense nuclear medium there then appears a strongly bound antinucleon, which lowers the baryon density and allows production of nucleon-antinucleon pairs as long as that density does not drop below critical, while a slow nucleon drifting to infinity appears in the vacuum. Analysis of this instability mechanism is supplemented with numerical estimates based on available and new data. The author thanks L. M. Satarov for fruitful discussions. Figures 2; tables 1; references 16.

Expansion of Effective Radius for dt-Scattering and $dt \rightarrow n\alpha$ Fusion

917J0050A Moscow YADERNAYA FIZIKA in Russian Vol 52 No 6(12), Dec 90 pp 1540-1557

[Article by B. M. Karnakov, V. D. Mur, and S. G. Pozdnyakov, Moscow Institute of Engineering Physics, and V. S. Popov, Institute of Theoretical and Experimental Physics at State Committee on Use of Atomic Energy]

[Abstract] A model-independent description of dt-scattering and $dt \rightarrow n\alpha$ fusion is obtained by expansion of the effective radius for each of these processes, as has been done for the one-channel problem of Coulomb interaction distorted within the short range. First the low-energy parameters of dt-scattering are calculated by this method, considering also that existence of $^3\text{He}^*(3/2^+)$ low-energy resonance in the system is responsible for the peculiarities of this process and that the $l = 0$ resonance mode plays the dominant role in both processes. The amplitude of elastic dt-scattering is then calculated accordingly without inclusion of other resonance modes and the analytical structure of the S-matrix is determined including the positions of its poles. Both

the Coulomb scattering length and effective radius have been obtained from experimental data on the cross-section for fusion and the differential cross-section for elastic scattering. The results are compared with three known models using the effective radius approximation: the model based on the R-matrix with "off resonance" levels added, the dynamic model with coupling of the dt-channel and the $n\alpha$ -channel through an intermediate nucleus, and the simplest optical model of strong dt-interaction. As short-range potential in the simplest model of strong interaction admitting an analytical and thus exact solution for all resonance modes $l = 0, 1, 2, \dots$ is selected the delta-function potential $V_s(r) = -(g/2R)\delta(r - R)$. The authors thank L. I. Bogdanova, V. Ye. Markushin, and G. M. Hale for helpful discussions. Figures 5; tables 4; references 32.

Measurement of Spectrum of Electron Antineutrinos From Nuclear Reactor

917J0050B Moscow YADERNAYA FIZIKA in Russian Vol 52 No 6(12), Dec 90 pp 1574-1582

[Article by Yu. V. Klimov, V. I. Kopeykin, A. A. Labzov, L. A. Mikaelyan, K. V. Ozerov, V. V. Sinev, and S. V. Tolokonnikov, Institute of Atomic Energy imeni I. V. Kurchatov]

[Abstract] Measurements of the e-antineutrino spectrum are being made in the underground neutrino laboratory, 18 m away from the center of the 1375 MW water-cooled water-moderated power reactor at the Rovno nuclear power plant. They are made using the two new detectors of the $\nu_e + p \rightarrow n + e^+$ reaction installed in 1987-89, a water integral detector and the small integral one, as well as the recently developed Rovno scintillation-type neutrino spectrometer containing two parallel specular reflectors and six FEU-125 photomultipliers. A liquid organic scintillator doped with gadolinium placed between the two mirrors serves as the target for antineutrinos, only a 510 dm³ large center core of this target having been used in the recent experiment. Events of the $\nu_e + p \rightarrow n + e^+$ reaction are isolated by applying the method of delayed coincidences to capture of neutrons in gadolinium between that of positrons and γ -quanta, 1000 events at nominal reactor power having thus been recorded in a total time of 10^5 s (27.8 h) over a period of seven months. The e-antineutrino spectrum in absolute units (MeV⁻¹/fission) was determined from 24 points on the histogram and using the reaction cross-section $\rho = (5.80 \pm 0.17) \times 10^{-43}$ cm²/fission, as measured in the same flux with the water integral detector. This spectrum is compared with the standard antineutrino spectrum $\rho(E_{\nu_e})$ of the reactor and with its positron spectrum. On the basis of already available data, the cross-section for the $\nu_e + p \rightarrow n + e^+$ reaction is compared with that for the $\nu_e + d \rightarrow n + p + \nu_e$ reaction in the neutral-current channel and with that for the $\nu_e + d \rightarrow 2n + e^+$ reaction in the charged-current channel. The authors thank S. A. Fayans and M. D. Skorokhvatov for helpful

discussions, S. V. Yegorov and A. G. Vershinskiy for participation in setting up the experiment. Figures 5; tables 4; references 30.

Possibility of Measuring Energy of Tritium β -Decay Edge by X-Ray Spectroscopy

917J0054A Tallinn IZVESTIYA AKADEMII NAUK
ESTONII: FIZIKA, MATEMATIKA Vol 39 No 4,
Oct-Dec 90 pp 353-357

[Article by Ain Ainsaar, Institute of Chemical Physics and Biophysics, Estonian Academy of Sciences]

UDC 539.123.6

[Abstract] A method of measuring the energy of the tritium β -decay edge with an x-ray spectrometer and thus more precise than with an ion-cyclotron-resonance spectrometer is proposed, tritium being for this purpose dissolved in palladium so that x-ray bremsstrahlung will be generated and emitted as higher-energy β -decay electrons strike Pd atoms. The x-ray spectrum will contain peaks corresponding to equal x-quantum and electron energy levels. Palladium has been selected because its atoms ($Z = 46$) have a large cross-section for generating x-rays, because its K-level (24.349 keV) is slightly above the energy level of the spectrum edge to be measured so that fewer x-quanta are absorbed while noise is absorbed, and because it can take a large charge of tritium. The advantages of an x-ray spectrometer are that x-quanta become either completely or not at all absorbed by the medium through which they pass and thus do not lose their energy gradually, that there is no need for shielding against electric and magnetic fields, also no need for a vacuum, and that the cost depends linearly on the size of the x-ray source. Its drawbacks are that each electron energy level covers a wide range of the x-ray spectrum, that its Pd-target must be thin and have a large surface so as to minimize energy absorption in it, and that its sensitivity to background radiation increases with its size. Considering that the edge of the tritium β -decay spectrum is 18.6 keV in terms of energy or 0.0667 nm in terms of wavelength and that 0.07 nm x-rays penetrate palladium 0.026 mm deep, the Pd-target must not be thicker than 0.05 mm. The half-life of tritium being 4×10^8 s, its β -decay activity in a Pd-target is estimated theoretically for 0.03 mm thick and 100 cm square sheet of palladium charged with 4×10^{21} ^3H molecules (1.5×10^{-2} m³ gas under normal pressure). The intensity of emitted x-rays covering a continuous spectrum and generated by monoenergetic electrons is theoretically estimated as $cZ(v_0 - v)$ ($Z = 46$, $c = 5.0 \times 10^{-57}$ J.s², v_0 - shortwave edge of x-rays, v - unit frequency band corresponding to a single electron). A crystal-grid spectrometer is thus shown to be feasible, its vertical (or horizontal) dimension limiting the beam scattering in that direction and the required precision limiting the beam scattering in the other direction. Shielding against background interference of cosmic origin requires that it be buried 5 km or deeper underground, which will still leave

γ -ray background interference. The spectrometer precision with a $1 \times 100 \times 100$ mm³ Ge(Li) detector with a 0.3 keV energy resolution can be as high 150 eV. It is possible to make it still higher, by improving the energy resolution of the Ge(Li) detector and by selecting a site where the level of natural radioactivity is low. The author thanks E. Lippmaa and E. Realo for helpful discussions. References 13.

Measurement of Ultrashort Dephasing Time in Extrinsic Glasses With Noncoherent Laser Pulses

917J0054B Tallinn IZVESTIYA AKADEMII NAUK
ESTONII: FIZIKA, MATEMATIKA in Russian Vol 39
No 4, Oct-Dec 90 pp 365-371

[Article by Rein Kaarli and Margus Ratsep, Institute of Physics, Estonian Academy of Sciences]

UDC 535.33

[Abstract] The method of scattering by light-induced spectral gratings was used for measurement of ultrashort dephasing time in two extrinsic polystyrene glass films doped with octaethyl porphine ($d = 0.5$ mm thick, optical density $D = 0.6$) and with H₂-4-tert-butyl porphyrizine ($d = 0.2$ mm thick, optical density $D = 1.4$) respectively. Both were excited with pulses of noncoherent light from a dye laser emitting radiation within the $\lambda = 610 - 620$ nm band in pulses of 10 ns duration. The active medium of this laser, a mixture of rhodamine 6G and 6-aminophenalenon, was pumped by a XeCl excimer laser. A glass film was kept in a He-cryostat at a temperature about 2 K. In a Michelson interferometer the laser beam was split into two, the reflected one passed through a fixed delay line (Porro prism) and then a polarizer, the transmitted one passed through an adjustable delay line (Porro prism) and then a polarizer, to a converging lens which focused both onto the glass film with a $(k_1, k_2) = 2^\circ$ angle between their wave vectors and a variable delay time. The peak power density within the laser spot on the glass film was 5-10 kW/cm². Upon leaving the glass film after having induced a spectral grating in it, each proceeded through a diaphragm to a photomultiplier. The delay time was varied by regulating the adjustable delay line in each direction, but only within the subpicosecond range so as to keep it much shorter than the duration of each pulse and the measurable dephasing time. The tail part of the delayed second pulse, scattered by the already induced spectral grating, could then be used for probing. Tests were performed with $\Delta\lambda = 1.2$ nm, 2.4 nm, and 8-10 nm (maximum) wide emission lines, corresponding to a coherence time of 0.94 ps, 0.46 ps, and 110-130 fs respectively. The autocorrelation function of such pulse pairs was measured by the method of noncollinear second-harmonic generation with a KDP crystal. Tests with H₂-4-tert-butyl porphyrizine were also performed at room temperature, but required a power density of at least 100 kW/cm² and a delay time not longer than the coherence time for excitation. The electric output signals from both photomultipliers were sent through a common

strobing amplifier to a recording instrument. The intensity of both $k_3 = 2k_2 - k_1$ and $k_4 = 2k_1 - k_2$ pulses and thus their attenuation in both glass films was found to depend on the time noncoherence of incident radiation and thus on the spectral width of incident pulses. Evidently, therefore, the characteristics of an extrinsic glass which determine dephasing of incident light pulses depend also on the spectral width of these pulses. For a more precise interpretation of the results of this study, they are compared with known results of spectral hole burning experiments. The authors thank P. Saari for interest and helpful discussions. Figures 4; references 18.

Structural Electron Microscopy of 08Mn2Si Steel Wire Drawn With Electrical Stimulation

917J0056A Tomsk IZVESTIYA VYSSHIKH
UCHEBNIKH ZAVEDENIY: FIZIKA in Russian
Vol 33 No 12, Dec 90 pp 31-35

[Article by V. Ye. Gromov, Yu. F. Ivanov, G. V. Pushkareva, Yu. P. Sharkeyev, E. V. Kozlov, L. B. Zuyev, and V. Ya. Tsellermayer, Institute of Strength Physics and Materials Science, Siberian Department, USSR Academy of Sciences, Tomsk Institute of Construction Engineering, and Siberian Institute of Metallurgy imeni S. Ordzhonikidze]

UDC 669.71:539.382.2:539.376:539.39

[Abstract] An experimental study of steel wire drawing with stimulation by short strong pulses of nonthermal electric current was made, for an analysis of the plastic deformation process and evaluation of this high-productivity technology. Welding wire of 08Mn2Si steel annealed at 680°C for 10 h was drawn by application of electric current pulses equivalent to a 750 MA/m² magnitude at a repetition rate of 150 Hz. At a pulling speed of 0.34 m/s, the wire was reduced from a 5.95 mm diameter to a 3.14 mm diameter in five passes: 5.95 → 5.18 → 4.48 → 3.90 → 3.65 → 3.14 mm corresponding to 14 → 28 → 42 → 49 → 64 percent reduction. The hot-spot temperature, measured with a special infrared transducer, never exceeded 180°C. The microstructure of this wire evolving in the process was examined under two transmission electron microscopes, a BS-540 and an EM-125, on 0.2 mm thick plates cut from the wire along and across the direction of pull. The plates were ground down to 0.1 - 0.05 mm thick foils and these were then electrolytically polished with a CrO₃ solution in H₃PO₄ under a voltage of 25-30 V. For an analysis of the microstructure, the volume fraction of fragments, their longitudinal and transverse dimensions, the azimuthal orientation diversity of neighboring fragments, and the scalar dislocation density were measured. On the basis of these measurements were determined the structural changes affecting the three component phases of this steel: ferrite (original volume fraction 0.75), lamellar and globular pearlite (original volume fraction 0.17), and martensite (original volume fraction 0.08). The microstructure of pearlite was found to change as it does

during conventional drawing, but oblong regions with an ultrafine dispersion to form during earlier stages of the reduction process. The volume fraction of pearlite was found not only to decrease appreciably, down to a final 0.05, thus much more than to a final 0.1 during conventional drawing, but also during the first two passes (28 percent reduction). Similarly the volume fraction of fragments was found to change as it does during conventional drawing, but becomes larger during the third pass (42 percent reduction) and then smoothly increases further to a final 0.95 (64 percent reduction). The scalar dislocation density was found to change differently than during conventional drawing, when it rises to a saturation level, namely rising during the first two passes to a maximum at 35 percent reduction and then dropping slightly during subsequent passes. The dimensions and the orientations of fragments, ferrite fragments, were found not to have changed during electrically stimulated drawing. While the orientation diversity of fragments was the same as after conventional drawing, the range of their sizes remained narrower. The authors thank V. Ye. Panin for stimulating their interest in this study. Figures 3; tables 1; references 10.

Anomalous Temperature Dependence of Lower Critical Magnetic Field for High-T_c Superconductor Ceramic

917J0059C Moscow PISMA V ZHURNAL
EKSPERIMENTALNOY I TEORETICHESKOY
FIZIKI in Russian Vol 53 No 2, 25 Jan 91 pp 93-96

[Article by M. A. Baranov, V. S. Gorbachev, and A. V. Senatorov, Moscow Institute of Engineering Physics]

[Abstract] A model of high-T_c ceramic superconductors is constructed for calculating the temperature dependence of the lower critical magnetic field H_{c1}(T) which, unlike the two-dimensional model applicable to weak-link materials in weak magnetic fields, covers the entire temperature range from T = 0 to the critical coherence transition temperature T_{cj}. The model is based on Hamilton's energy functional for a cubic lattice of grains in a Josephson medium and its extension to the continuous-medium limit. It involves only the intergranular contact energy E_j and the magnetic energy of grains but not spin glass properties of a disordered system with a random distribution of contact energy. The effective Hamiltonian and the statistical sum $Z = e^{-(F/T)}$ (F - free energy in a statistical system) are calculated with the aid of the Hubbard-Stratonovich identity, by virtue of which integration over the θ (phase) field can be replaced with integration over the ψ (order parameter) field. For an order parameter $|\psi| \ll 1$, near the T_{cj} temperature, series expansion of the nonlinear term in the expression for the effective Hamiltonian leads to the Ginzburg-Landau model and variational treatment of the effective Hamiltonian yields an equation for the mean field. Expressions for the field penetration depth δ , the coherence length ξ , and the lower critical magnetic field H_{c1} are obtained from this equation in the mean field approximation involving the thermodynamic mean of

the order parameter. The temperature dependence of the lower critical field $H_{c1}(T)$ is then evaluated accordingly, and taking into account the temperature dependence of the contact energy, this energy being usually much lower at the T_{c1} temperature than at $T = 0$. Calculations reveal an anomalous trend of the $H_{c1}(T)$ dependence, namely a falling of H_{c1} by inflection from its higher value at $T = 0$ to its lower value at the critical superconducting transition temperature T_{cg} for grains. This trend characterizes SNS junctions and SIS junctions with a small coherence length but not other SIS junctions. An experimental verification is difficult because of the very weak lower critical field, but measurements made on 123-phase $YBa_2Cu_3O_x$ ceramic have also revealed such an inflection. Figures 1; references 10.

Correlated Acoustic and Neutron Emission From Deuterium-Impregnated Palladium Target

917J0059D Moscow PISMA V ZHURNAL
EKSPERIMENTALNOY I TEORETICHESKOY
FIZIKI in Russian Vol 53 No 2, 25 Jan 91 pp 115-118

[Article by P. I. Golubnichiy, A. D. Filonenko, and A. A. Tsarik, Lugansk Institute of Machine Construction; V. V. Kuzminov and B. V. Pritychenko, Institute of Nuclear Research, USSR Academy of Sciences, Moscow; G. I. Merzon and V. A. Tsarev, Institute of Physics imeni P. N. Lebedev, USSR Academy of Sciences, Moscow]

[Abstract] Experiments were performed in the low-noise chamber of the Baksan underground laboratory at a water equivalent depth of 1000 m, their purpose was to verify the earlier predicted existence of a time correlation between pulses of neutron emission and acoustic

emission from palladium during its electrolytic impregnation with deuterium. A bar of 99.9 percent pure palladium $2.5 \times 5 \times 56 \text{ mm}^3$ large having an active surface area of 2.5 cm^2 and a mass of 10 g was used as the cathode with a platinum anode of an open electrolyzer containing 20 ml of $0.1 \text{ mol./dm}^3 \text{ LiClO}_4$ solution in D_2O . Neutrons produced in the $d, d \rightarrow {}^3\text{He}, n$ reaction were slowed down in a paraffin block and then recorded with 10 SNM-18 counters. The recording efficiency was approximately 10 percent, based on separate measurements with Pu-Be and ${}^{252}\text{Cf}$ neutron sources. Acoustic emission signals corresponding to the neutron emission pulses in accordance with the deutron acceleration model (neutrons being produced by collisions of deuterons upon their acceleration in the electric field of charges generated during spallation of impregnated palladium) were measured with an acoustic transducer. The time differences between recording a neutron emission and an acoustic emission $\Delta t = t_a - t_n$ (t_a - time taken by acoustic signal to pass through target, t_n - time taken for slowdown of neutrons) were measured on the screen of an oscillograph. The total duration of the experiment was 8.5 h, with the density of the electrolyzer current varied over the 10 - 60 mA/cm² range and included 3.5 h of correlation measurements. After approximately 5 h the rate of neutron count had increased to twice the background count, neutron emission having then also been recorded upon quenching of the target in liquid nitrogen. Altogether 42 events were recorded, the time correlation between neutron emission and acoustic emission being within 100 μs and $\Delta t < 0$. The results confirm the existence of that time correlation and agree with the acceleration model of cold fusion. The authors thank A. A. Pomanskiy for collaboration and Professor M. Danos for helpful discussions. Figures 3; references 4.

Measurement of Optical Rotation Angle With Subnanosecond Time Resolution

917J0045C Tomsk IZVESTIYA VYSSHIKH
UCHEBNIK ZAVEDENIY: FIZIKA in Russian
Vol 33 No 9, Sep 90 pp 34-39

[Article by M. V. Arkhipov, S. V. Pavlov, and N. S. Ryazanov, Institute of Physics at Leningrad State University]

UDC 535.56

[Abstract] A method of measuring the angle of optical rotation within the duration of an incident nanosecond radiation pulse with a time resolution of 0.5 ns or better is described, such a resolution was attained with one common photodetector for both measuring channels and with time division of channels by optical rather than electrical means. The method is demonstrated on rotation of the polarization plane of radiation while an optically active device is being placed in the optical cavity of a pulse dye laser. The method is designed for real-time recording of the rotation angle throughout the transient period. The apparatus includes a Frank-Ritter birefringent polarizing prism which splits the incident light beam into two with mutually orthogonal linear polarizations. One of these beams passes through a polarizer before entering an F-28 pulsed photocell in a coaxial connection which ensures a time resolution of 0.3 ns. The other beam travels along an optical delay line formed by plane mirrors before entering the same photocell, the path of the delayed beam being sufficiently long for the delay time to exceed the duration of the radiation pulse. The radiation intensity in both channels can be varied and optical losses in the delay line can be compensated by means of that polarizer. A diffuser plate in front of the photocell ensures that the latter is uniformly illuminated and minimizes the effect of nonuniform photocathode sensitivity on the magnitude of the electric photocell output signal. A focusing lens behind the last delaying mirror ensures that the areas of the two light spots on the diffuser are approximately equal. The electric signal from the photocell proceeds through a 20 cm long cable to the deflection plates of a S7-10B high-speed cathode-ray oscillograph. The performance of the recording apparatus, in the general case of partly polarized radiation, can be described in terms of the Jones matrix. Its threshold sensitivity is 8 mrad, adequate for monitoring the dynamics of optical rotation in real-time intracavity laser polarization spectroscopy. Figures 4; references 9.

Channeling and Collimation of and Radiation Emission by Relativistic Electrons in Nonuniform Superhigh-Intensity Light Fields

917J0057A Moscow PISMA V ZHURNAL
EKSPERIMENTALNOY I TEORETICHESKOY
FIZIKI in Russian Vol 53 No 1, Jan 91 pp 18-20

[Article by A. V. Andreyev and S. A. Akhmanov, Moscow State University imeni M. V. Lomonosov]

[Abstract] Interaction of relativistic electron beams and nonuniform superhigh-intensity coherent-light fields is analyzed theoretically, the simplest example of such a field being that of interfering two superposed plane light waves. The analysis is based on the equation of transverse motion for electrons in a beam propagating parallel to the antinodes of such an interference field, assuming that the field has only a transverse electric component and two mutually orthogonal magnetic ones. When the frequency $\Omega = eE_0 \sin \theta / 2^{1/2} mc$ is much lower than $\omega (1 - \beta \cos \theta)$ (E_0, θ - electric field intensity and frequency waves, e, m - charge and mass of electron, c - speed of light, θ - angle between wave vectors k_1, k_2 and z - direction of electron beam propagation, β - beta factor), then the motion of these electrons is shown to be a superposition of low-frequency oscillations with an amplitude a_Ω and high-frequency oscillations with an amplitude $a_\omega \ll a_\Omega$. Also when the energy of their transverse motion is lower than the potential barrier $U_0 = (eE_0)^2 / 4m\omega^2$, then their oscillations are confined between two antinodes. The critical angle for such a channeling of electrons is $\eta = eE_0 / 2^{1/2} m\omega c$. Transverse oscillations of electrons give rise to Doppler branches of radiation emission at an angle γ to the direction of electron beam propagation. At parametric resonance $\Omega = \omega(1 - \cos \theta)$ the amplitude of transverse oscillations should increase, but radiation emission by transversely oscillating electrons will attenuate it when the beam-field interaction time is much longer than the attenuation time. In this case a relativistic electron beam will be also collimated. Figures 1; references 3.

Anomalies in Spectral-Angular Distribution of γ -Radiation Emission by Ultrarelativistic Electrons in Thick Crystals

917J0057B Moscow PISMA V ZHURNAL
EKSPERIMENTALNOY I TEORETICHESKOY
FIZIKI in Russian Vol 53 No 1, Jan 91 pp 51-54

[Article by A. P. Antipenko, S. V. Blazhevich, G. L. Bochek, V. I. Kulibaba, N. I. Maslov, N. N. Nasonov, V. D. Ovchinnik, S. P. Fomin, B. I. Shramenko, and N. F. Shulga, Institute of Engineering Physics, UkSSR Academy of Sciences, Kharkov]

[Abstract] Generation of γ -quanta in a thick crystal upon passage of an ultrarelativistic electron beam along one of the crystallographic axes is considered and a method of measuring the true spectral-angular distribution of 0.1 - 600 MeV γ -quanta in a high-intensity flux is proposed, in measurements by conventional methods all γ -quanta being lumped into a single one with the sum total energy. The new method, based on Compton scattering of emitted γ -quanta, involves measuring, with a total-absorption spectrometer, the energy of those scattered a certain angle. Measurements by this method were made in the LU-2000 accelerator at the Kharkov Institute of Engineering Physics. The apparatus consisted of a target, a goniometer, a deflecting electromagnet, a photon flux collimator, a scrubbing electromagnet, a beryllium target acting as scatterer, an ionization chamber, a lead block,

a γ -flux collimator, another scrubbing electromagnet, two more γ -flux collimators, a scrubbing magnet, a total-absorption scintillation spectrometer in a protective housing, and a protective concrete wall. The angular resolution of the measuring apparatus was ± 0.00015 rad. Silicon crystals of various thicknesses were oriented with their 111 axes along a 1.2 GeV electron beam, for measuring spectral-angular intensity distributions of the radiation emitted by electrons and of the γ -radiation. In the range of low-energy γ -quanta (up to 10 MeV) the intensity of radiation emission by electrons was over 20 times higher along the crystallographic axis than in a not so oriented crystal, thus higher by a factor much larger than in earlier experiments. The difference can be explained by the different methods of measurement, the true spectral-angular radiation intensity distribution having been measured here while the integral photon yield within some energy range of γ -quanta was measured earlier. In this range, moreover, the width of the angular distribution of γ -quanta was almost independent of the photon energy. In the range of high-energy γ -quanta (from 50 MeV up) the radiation intensity was minimum along the crystallographic axis and maximum radiation intensity at some angle to it, the angle being larger for γ -quanta with higher energy. In this range the angular distribution of γ -quanta widened as the photon energy increased. The results of these measurements confirm theoretical predictions regarding the radiation emission by electrons in thick crystals and thus validate the hypothesis that its spectral-angular distribution is determined by the characteristics of coherent radiation emission by suprabarrier electrons moving through the field of the atomic chain within the paraxial region. Figures 2; references 9.

Possibility of Producing New Integrated-Optics Polarizers and Waveguide- Mode Transformers

917J0058C Leningrad PISMA V ZHURNAL
TEKHNICHESKOY FIZIKI in Russian Vol 16 No 24,
26 Dec 90 pp 73-77

[Article by A. A. Voyevodin, V. P. Gladkiy, I. A. Prokhorova, and N. A. Yakovenko, Kuba State University]

[Abstract] An experimental feasibility study of new integrated-optics devices consisting of channel waveguides diffused into passive substrates was made, such a device acting as polarizer of optical TE or TM modes depending on the width of the transparent film which covers a segment of the channel waveguide. The width of this film must be sufficiently small to prevent generation of a given waveguide mode directly in it and its thickness for transmission of a TE mode h_E must be smaller than h_M is necessary for transmission of a TM mode. When the thickness of this film is not uniform but varied along the waveguide from h_E to h_M , then the device becomes a TE \rightarrow TM mode transformer. Channel waveguides with an effective refractive index 1.572 for 0.6328 μ m light were formed in substrates of K-8 optical glass with a refractive index 1.5136, by the ion-exchange process in KNO_3

melt. They were then covered with film of glassy As_2S_3 by the vacuum deposition process, the refractive index of this chalcogenic glassy semiconductor being 2.5 and thus much larger. The devices were tested for polarization of both TE_{00} and TM_{00} modes as well as for transformation from one to another, with a 20 - 25 dB decoupling between these two orthogonal modes and a 1.5 - 2 dB optical insertion loss during passage of a transformable mode through a 2 mm thick transparent film. The experiment has confirmed the feasibility of fine-tuning the parameters of such polarizers and mode transformer for optimum performance by using transparent films of chalcogenic glassy semiconductors and the change of optical characteristics upon exposure to light of resonance wavelength. This was demonstrated by an increase of the decoupling between orthogonal optical modes up to 3 dB upon exposure to 0.47 μ m light with a power density of 100 mW/cm², 0.47 μ m being the resonance wavelength for As_2S_3 films. Figures 3; tables 1; references 3.

Quantum Fluctuations Annihilate Optical Soliton

917J0059A Moscow PISMA V ZHURNAL
EKSPERIMENTALNOY I TEORETICHESKOY
FIZIKI in Russian Vol 53 No 2, 25 Jan 91 pp 73-76

[Article by A. V. Belinskiy, Moscow State University imeni M. V. Lomonosov]

[Abstract] Formation of an ideal fundamental soliton which satisfies the nonlinear Schroedinger equation and propagates through an infinitely long nonlinear optical fiber is considered, its "self-cleansing" from classical fluctuations was shown not to compensate the increase of quantum fluctuations upon its passage into the far region but rather to let it become finally annihilated by the increasingly destabilizing effect of quantum indeterminacy. Analysis of this problem is based on the nonlinear Schroedinger equation with the Heisenberg representation of both photon generation and annihilation operators $\phi^+(x,t), \phi(x,t)$ (x - distance, t - normalized time) which describes evolution of a quantum field in a fiber with cubic nonlinearity. For description of the soliton envelope, both operators are reduced to the Schroedinger representation $\phi^+(x), \phi(x)$ and the state vector $|\psi\rangle$ is transformed so as to satisfy the Hamiltonian of the system. The envelope as a superposition of Fock states $|n,p\rangle$ (n - number of photons, p - momentum) is shown to become wider and its amplitude lower in time so that the soliton eventually vanishes. This result is explained with the aid of the model of a soliton envelope entering an optical fiber as an ensemble of coherent modes with a different amplitude each and quantum fluctuation in the fiber superposing on its sech envelope as vacuum noise. Following linearization of the nonlinear Schroedinger equation with respect to fluctuation states, single-mode interaction is considered for simplicity and the noise intensity is shown to increase as a consequence of four-photon interaction resulting in transition of photons from regular soliton component to its fluctuation component. This explanation is supplemented with

numerical estimates of maximum soliton propagation time with minimum blurring of a soliton in an optical fiber with a nonlinearity parameter c such that $|c| \leq \Delta p$ and the soliton can be regarded as a classical one. The author thanks V. A. Vysloukh for helpful discussions. Figures 1; references 7.

Generating High-Intensity Radiation Fluxes and Megabar Pressures in Liner Systems

917J0059B Moscow PISMA V ZHURNAL
EKSPERIMENTALNOY I TEORETICHESKOY
FIZIKI in Russian Vol 53 No 2, 25 Jan 91 pp 83-86

[Article by V. A. Gasilov, S. V. Zakharov, and V. P. Smirnov, Institute of Atomic Energy imeni I. V. Kurchatov, Troitsk branch (Moscow Oblast)]

[Abstract] A plasma liner system for generating short pulses of high-intensity soft x-rays and up to gigabar pressures is described, such a liner consisted of a plasma sleeve around a coaxial solid rod with a 10 times smaller diameter. The sleeve is accelerated by pressure of the magnetic field, its velocity reaching 300-500 km/s while

it is compressed till it collides with the rod. As it stalls, its kinetic energy is converted into radiation and its momentum produces a pressure pulse which adds to the pressure of the magnetic field. The amplitude of resulting Rayleigh-Taylor instability is limited by finiteness of the compression ratio, approximately 10:1. Subsequent interaction of the plasma sleeve and the plasma corona around the rod causes the thickness of the sleeve to decrease and the plasma density in it to increase so that the pulse of soft x-rays becomes shorter while the amplitudes of both radiation intensity and pressure increase. The process involving a xenon sleeve (initial radius $R = 1.65$ cm, linear mass $M/L = 140$ $\mu\text{g}/\text{cm}$) and a molybdenum rod (diameter $d = 2$ mm) was simulated on a computer using the RAZRYAD (DISCHARGE) program package. Calculations were made for such a liner carrying a current of 2.5 MA amplitude in the sleeve, the latter being accelerated to a velocity $V = 400$ km/s and compressed to collision with the rod. Taken into account was nonisothermality of the plasma during acceleration. The author thanks A. Yu. Krukovskiy and K. V. Skorovarov for assisting with the calculations. Figures 2; references 7.

Outlook for Practical Use of Thermonuclear Fusion With Magnetic Plasma Confinement

917J0034A Moscow FIZIKA PLAZMY in Russian
Vol 16 No 12, Dec 90 pp 1397-1409

[Article by I. N. Golovin, Institute of Atomic Energy imeni I. V. Kurchatov]

UDC 533.951

[Abstract] The problem of curtailing combustion of organic fuels for ecological purposes such as abatement of the warming effect due to accumulation of CO_2 and other hotbed gases in the atmosphere without depressing the world's economy is analyzed from the long-range viewpoint reaching up to the year 2050. Following a review of the status of nuclear power based on nuclear fission and solar power with emphasis on their drawbacks, radiation hazard and waste disposal problems in the first case, high cost of equipment and prohibitively large surface areas in the second case, thermonuclear power based on nuclear fusion is seen as a third alternative. Particularly attractive from both ecological and economical standpoints is controlled fusion with magnetic plasma confinement, if sufficiently compact, efficient, and reliable, and low-cost fusion reactors can be built for safe operation with minimal radioactive fallout and possibly with fail-proof features. Two basic kinds of fusion reactors are under consideration: 1) D-T reactors (ITER, NET), operating at not much lower radioactivity levels than do conventional pressurized-water reactors but not breeding long-lived toxic nuclides such as Cs or Sr isotopes, also inherently incapable of uncontrollable runaway inasmuch as the reaction slows down during breakdown; 2) D- ^3He low-radioactivity reactors, featuring a long-lived first wall adequate for over 100 years of service. While selection of structural materials for a D- ^3He reactor does not present a difficult problem, in view of the relatively mild performance criteria, availability of helium is a serious problem on account of its scarcity in the earth and in the atmosphere so that other means of acquiring it must be sought. These include β -decay of tritium, helium being thus produced in the Canadian CANDU heavy-water uranium reactor. Noteworthy is the great abundance of helium on the moon and on other planets such as Jupiter, having been acquired by them from solar winds over a period of billions of years. The energy requirement for its acquisition from the moon has already been estimated at the University of Wisconsin. This survey of the state of the art indicates that there is the need for: 1) a full-scale experimental study of plasma ignition in ITER and NET D-T reactors, 2) further conceptual tokamak design projects, 3) a new technology of producing structural materials with high activation resistance at conventional radiation levels and a search of materials with high activation resistance at high radiation levels up to 120 $\text{MW}\cdot\text{yr}/\text{m}^2$ fluence of 14 MeV neutrons, 4) a conceptual design of a lunar industry capable of delivering lunar He-3 to Earth. Figures 6; references 9.

Possibility of Cosmic Rays Being Generated in Plasma Pinches

917J0034B Moscow FIZIKA PLAZMY in Russian
Vol 16 No 12, Dec 90 pp 1457-1468

[Article by V. P. Vlasov, S. K. Zhdanov, and B. A. Trubnikov, Institute of Atomic Energy imeni I. V. Kurchatov and Moscow Institute of Engineering Physics]

UDC 533.6.952:539.12.164

[Abstract] The spectrum of galactic cosmic rays within the $E \approx 10^{10} - 10^{15}$ eV energy range, known to fit the relation $I(E) = dN/dE = AE^{-\nu}$ where $\nu = 1 + 3^{1/2} = 2.732$, is analyzed in terms of a hypothetical acceleration mechanism of their generation in a plasma pinch. A single almost cylindrical z-pinch with a full skin effect is considered, assuming that the plasma within it is described by the two Landau-Lifshitz equations of relativistic gas dynamics without a magnetic field. Introduction of the dimensionless linear density and stipulation of a pressure on the lateral pinch surface equal to the magnetic field pressure reduce these equations to a form which in the nonrelativistic approximation reduces them further to "quasi-Chaplygin" equations with an "azimuthal number" $m = -1$. These are solved first, assuming that the linear density of the plasma is an inverse-square function of the radial coordinate, before the original relativistic equations are solved. A spectrum of plasma jet ejection from the pinch is obtained on this basis which has almost the identical form as that spectrum of galactic cosmic rays and thus supports the hypothesis of their origin. Figures 3; references 19.

Microwave Breakdown of Atmospheric Air in Strong Light Fields

917J0034C Moscow FIZIKA PLAZMY in Russian
Vol 16 No 12, Dec 90 pp 1513-1516

[Article by I. V. Sokolov, Institute of General Physics, USSR Academy of Sciences]

UDC 537.533

[Abstract] The effect of visible and near-ultraviolet radiation on microwave electric breakdown of atmospheric air is analyzed, considering cold dry air under a pressure of about 1 atm. Microwaves generated by electric discharge in such air are assumed to have a frequency lower than that of electron-neutral collisions and an r.m.s. amplitude lower than the electric breakdown field intensity $E_b \approx 32$ kV/cm. The concentration distribution of electrons which have been generated here by any mechanism depends on intensity E of the microwave electric field, as do both the frequency ν_i of ionizing electron impacts and the much higher frequency ν_a of electron-molecule attachments. The air is also considered to be in the field of radiation with a quantum energy not exceeding 6 eV, below the ionization potential, and with

an intensity far below the optical breakdown threshold. The condition for electric breakdown, namely electron avalanche, is established and the dispersion relation is derived by solving the equation of kinetics for the electron concentration in air. This equation includes terms which account for photodetachment of electrons from $O_{1,2,3,4}^-$ ions: O^- and O_2^- ions having been formed by dissociative or three-particle attachment, O_3^- and O_4^- ions having been formed by ion conversion. Relevancy is during the initial stage of ion conversion, when the electron concentration is still low, so that only interactions with cold unexcited O_2 and N_2 molecules need to be considered. On this basis the $E > E_b$ criterion for electric breakdown is shown to be equivalent to an electron-to-molecule attachment frequency $\nu^* > \nu_{a1} + \nu_{a2}$ (frequencies of electron attachments to atmospheric oxygen resulting in formation of O^- and O_2^- ions respectively). Radiation influences electric breakdown appreciably only when its quantum energy exceeds 2 eV so that in this case an impact ionization frequency higher than needed for overcoming diffusion losses only and not diffusion losses plus attachment losses is sufficient for a positive avalanche constant. The author thanks S. V. Bulanov, I. A. Kossov, A. Yu. Kostinskiy, and V. P. Silakov for discussions and consultations. Figures 1; references 11.

Transport of Relativistic 100 kJ Microsecond Electron Beam Through Gas and Plasma in Strong Magnetic Field

917J0034D Moscow *FIZIKA PLAZMY* in Russian
Vol 16 No 12, Dec 90 pp 1147-1456

[Article by B. A. Knyazev, P. I. Melnikov, and V. V. Chikunov, Institute of Nuclear Physics, Siberian Department, USSR Academy of Sciences]

UDC 533.9.07

[Abstract] A series of experiments have been performed in the SPIN apparatus, the latest involving transport of a magnetized relativistic pulsed high-energy electron beam through vacuum, gas, and plasma. The apparatus consists of 1 m long solenoid which produces a quasi-steady magnetic field within a rise time of 12 ms to a strength of 4 T strength inside the solenoid and 8.8 T in the mirrors. The electron beam is transported from the accelerator successively through a foil anode, through a compartment where a magnetic field compresses it, then through a vacuum tube inside the solenoid, and finally through an expander to a graphite calorimeter inside a vacuum chamber which absorbs it. The vacuum tube is made of stainless steel and has an inside diameter of 104 mm. By admitting either air or helium, the density of the gas in all three compartments can be the residual level with a molecule concentration n_0 of about 10^{12} cm^{-3} to a level corresponding to n_0 of about $3 \times 10^{16} \text{ cm}^{-3}$. The electron beam in this experiment carried an energy of 100 J in pulses of 5 μs duration. Its current was measured with eight Rogowski loops at key locations and its energy

content was measured with that calorimeter. Lateral pressure of the plasma building up during transport of the electron beam was measured with three magnetic probes at key locations. The plasma density was measured with an infrared Michelson interferometer at the 3.39 μm wavelength. Radiation emission by the plasma was recorded by a 9-channel fiber-optic photomultiplier set, after the radiation had passed through an MDR-23 monochromator. The purpose of the experiment was to determine basic laws governing the transport of such an electron beam in a strong magnetic field, to determine the influence of the transport system on the performance of the accelerator diode and to thus detect a feedback effect, and to study charge and current neutralization as well as plasma generation and the conditions of energy transfer from beam to plasma in the compressor-solenoid-expander drift space. Actually three experiments were performed: 1) passage of electron beam through high-density neutral gas with $n_0 > 2 \times 10^{15} \text{ cm}^{-3}$ concentration, 2) passage of electron beam through low-density neutral gas with $n_0 < 10^{14} \text{ cm}^{-3}$ concentration, 3) passage of electron beam through plasma and medium-density gas with $n_0 = 6 \times 10^{14} - 2 \times 10^{15} \text{ cm}^{-3}$ concentration. The data reveal two modes of plasma generation, by boundary-layer breakdown under low gas pressure and by volume ionization under high gas pressure, with some beam instability developing under low and medium gas pressures. They also indicate that a relativistic 100 kJ electron beam with a current density up to 2 kA/cm² can, within a pulse of 5 μs duration, be efficiently transported through a neutral gas and through an already existing plasma with an electron concentration n_e of about $1.2 \times 10^{15} \text{ cm}^{-3}$ in a 4 T strong magnetic field. The efficiency was higher when aluminum or dacron foils separated the solenoid cavity especially from the compression compartment. The authors thank Yu. I. Deulin and V. S. Nikolayev for building the SPIN apparatus, A. V. Burdakov, V. S. Burmasov, S. G. Voropayev, V. S. Koydan, S. V. Lebedev, D. D. Ryutov, A. D. Khilchenko, and M. A. Shcheglov for collaboration and helpful discussions. Figures 5; references 21.

Conditions for Effective Energy Radiation Into Plasma

917J0055B Kiev *UKRAINSKIY FIZICHESKIY ZHURNAL* in Russian Vol 35 No 12, Dec 90
pp 1822-1826

[Article by N. A. Zhizhnyak and N. M. Yatsenko, Kharkov University]

UDC 621.396.67:533.9

[Abstract] The problem of matching a linear antenna in a strongly magnetized plasma for effective radiation of energy into such a medium is analyzed theoretically, considering a nonideal dipole antenna with a radius r much smaller than its length L and than the radiation wavelength λ oriented at an arbitrary angle γ to the direction of the external magnetic field and thus to the

axis of anisotropy. The dielectric permittivity of the medium is described by a second-order tensor with only diagonal $\epsilon_1, \epsilon_1, \epsilon_3$ components in the Cartesian system of coordinates and its magnetic permeability is equated to unity. With a negative either ϵ_1 or ϵ_3 , the effective dielectric permittivity $\epsilon_{\text{eff}} = \delta^2 \cos^2 \gamma + \delta(\epsilon_1^{1/2}) \sin^2 \gamma$ ($\delta^2 = \epsilon_3 \sin^2 \gamma + \epsilon_1 \cos^2 \gamma$, can depending on the inclination angle γ of an ideal antenna, be either positive real ($\delta^2 > 0$) or complex with a negative real part ($\delta^2 < 0$). In the first case the antenna is tunable to resonance and in the second case it is nonresonant. An analytical expression for the antenna current arbitrarily induced in each case is obtained by the method of partial averaging from the equations of scattering for the general case of electromagnetic waves and dielectric bodies, with the internal impedance of the antenna and the wave number of electromagnetic radiation in the plasma as parameters. The relation between them at resonance is then established for a real symmetric dipole antenna in the form of two dispersion equations. Numerical calculations for such an antenna inclined at 90° to the external magnetic field in a plasma and excited by a plane electromagnetic wave E_0 in a plasma have yielded the dependence of the normalized antenna current $I(0)/(E_0/k_0)$ (k_0 - wave number in vacuum or isotropic free space) on the dipole length measured in wavelengths L/λ . The results are compared with the results of a laboratory experiment involving such an antenna in a plasma (electron concentration $n = 10^8 \text{ cm}^{-3}$, Langmuir frequency $\omega_N = 5.6 \times 10^8 \text{ Hz}$, Larmor frequency ω_B in a magnetic field of 3,500 Oe intensity). The dipole length was varied, while the wavelength of the exciting electric field and thus the plasma permittivity tensor were held constant. The results reveal that a real antenna with a purely imaginary surface impedance and an ideal one have a current-length characteristic with resonance in a plasma when $\delta^2 > 0$, both amplitude and width of the resonance peak depending on that impedance, while an ideal antenna is not resonant in a plasma when $\delta^2 < 0$. Figures 2; references 3.

Plasma Channel Formation in Nitrogen During Electron Beam Injection

917J0056B Tomsk IZVESTIYA VYSSHIKH
UCHEBNIKH ZAVEDENIY: FIZIKA in Russian
Vol 33 No 12, Dec 90 pp 58-59

[Article by V. P. Grigoryev and A. G. Potashev, Scientific Research Institute of Nuclear Physics at Tomsk Polytechnic Institute imeni S. M. Kirov]

UDC 533.95

[Abstract] The dynamics of a relativistic high-current electron beam propagating through a nitrogen-filled drift tube under high pressure and the attendant formation of a plasma channel are analyzed on the basis of experimentally verifiable models. These models include formation of complex ions, as a result of which the concentration of simple ions correspondingly decreases. This process is characterized by a rate constant $K_i \approx 5 \times 10^{-29}$

cm^6/s when $x < 4$ and $K_i = 4.6 \times 10^{-29} e^{2/3-x/6}$ when $x \geq 4$, where $x = (E_z/n_g) \cdot 10^{16} \text{ V} \cdot \text{cm}^2$ (E_z - axial component of electric field in drift tube, n_g - concentration of gas molecules in drift space). This process becomes noticeable as the pressure reaches the 50 - 70 torr range and, under pressure within the 100 - 760 torr range, may alone determine the annihilation of ions and electrons, inasmuch as complex ions recombine faster than simple ones. Ionization of the gas and neutralization of the electron beam upon axial injection of the latter are described by a system of three partial differential equations: 1) Poisson's equation for the resultant magnetic field potential A_z due to the sum of beam current and plasma current; 2) equations of kinetics for the concentration of complex ions and of simple ions. This system of equations has been solved numerically for a pulsed relativistic axisymmetric electron beam carrying trapezoidal current pulses into a cylindrical drift tube containing nitrogen, assuming ideal walls of the drift tube and with the boundary conditions for the magnetic field potential stipulated accordingly. For ionization is considered only the most interesting case of higher than 100 torr pressure and longer than 10 ns rise time of current pulses, in which case the electron temperature is approximately the same across the tube and the concentration of complex ions is approximately equal to the electron concentration. The initial conditions for neutralization are stipulated considering that, prior to complete neutralization, impact ionization of the gas in the drift space was effected not only by beam electrons but also by plasma electrons while the plasma was expanding. Figures 5; references 8.

Microwave Discharges in Stratosphere and Their Effect on State of Ozone Layer

917J0061A Moscow FIZIKA PLAZMY in Russian
Vol 17 No 1, Jan 91 pp 85-96

[Article by G. A. Askaryan, G. M. Batanov, I. A. Kossyy, and A. Yu. Kostinskiy, Institute of General Physics, USSR Academy of Sciences]

UDC 536.527:551.510.534

[Abstract] Formation of artificial ionized regions as plasma mirrors or ionospheric D-layer in the stratosphere by interaction of microwave radiation beams is examined, this being not only a problem of facilitating radio communication but also an ecological one in terms of consequences regarding the ozone layer. The problem is tackled theoretically by considering the possible plasmochemical reactions triggered by microwave discharges and involving nitrogen oxides NO_x ($x = 1, 2, 3$), which react with ozone O_3 but are recovered while ozone is reduced to oxygen O_2 . These reactions are analyzed quantitatively with the aid of available numerical data covering the relevant altitude range (35-80 km), thus also the corresponding temperature and pressure ranges. Such an analysis reveals that most effective in forming

artificial ionized regions may become electronic excitation of nitrogen molecules stimulating their oxidation $N_2^*(A^3\Sigma_u^+) + O \rightarrow NO + N(^2D)$ and $N(^2D) + O_2 \rightarrow NO + O$, breakup of oxide molecules $N(^2D) + NO \rightarrow N_2 + O$, also quenching of metastable nitrogen states $N_2^*(A^3\Sigma(\text{infu}^+ + O_2 \rightarrow N_2 + 2O$ and $N_2O + O$. Insofar as the buildup of nitrogen oxides is determined by the conditions under which an artificial ionized region is formed, it will depend accordingly on the magnitude of the parameter $\kappa \equiv E_e/n_m$ (E_e - effective electric field of wave, proportional to amplitude of discharge-sustaining electric field, n_m - concentration of molecules in atmosphere at the altitude of artificial ionized region). The ozone concentration in the stratosphere thus decreases as the excess NO concentration increases, such a depletion of ozone is shown to occur within several days already and most dangerous in this respect are shown to be high-(average)power microwave discharges occurring at 40 km altitude. These estimates are based on a system of 22 equations describing the kinetics of relevant chemical and photochemical reactions, this system of equations having been solved on a computer for typical microwave frequencies, angles between intersecting microwave beams, radio pulse repetition rates, wind velocities, and dimensions of an artificial ionized region. The results confirm earlier conclusions that microwave discharges cannot be expected to contribute to recovery of ozone. In order to refine and supplement the mathematical model, a laboratory experiment simulating the formation of an artificial region was designed and performed at the Institute of General Physics. A beam of 2 cm microwave radiation was injected into a vacuum chamber (diameter 35 cm) with metal walls in pulses of 0.2 J energy and 10 μ s duration at a repetition rate of 2 Hz, entering through a polystyrene lens which converged it into a 2 cm wide focal spot on a breakdown initiator discharge trigger inside an air-filled glass flask (diameter 14 cm) where the pressure was varied over the 70-760 torr range. Leaving the flask behind, the beam diverged while proceeding toward a radiation absorber along the back wall of the chamber. Through a lateral quartz window in the chamber, a probing beam of ultraviolet radiation from a mercury lamp was injected, this beam crossing the microwave beam inside the flask and then being focused by another lens onto the slit of an MDR-3 monochromator behind another lateral quartz window in the chamber. Radiation of a mercury lamp had been selected for monitoring the ozone content in air along with the buildup of nitrogen oxides, considering that 400 nm radiation would be largely absorbed by NO_2 while 200 - 300 nm radiation would be only slightly absorbed by nitrogen oxides. The ozone concentration could thus be estimated on the basis of the optical absorption coefficient in the flask. The results of this experiment confirm the results of theoretical analysis. The magnitude of the specific energy input, per molecule, into formation of an artificial ionized region by interaction of microwave

beams is thus shown to make this a method, its formation ecologically detrimental in terms of ozone layer depletion. Figures 5; references 27.

Theory of Microwave Discharge in Low-Pressure Gas

917J0061B Moscow PISMA V ZHURNAL
EKSPERIMENTALNOY I TEORETICHESKOY
FIZIKI in Russian Vol 17 No 1, Jan 91 pp 97-101

[Article by Yu. R. Alanakyan, "Gorizont" (Horizon) Experimental Engineering Office]

UDC 533.9:537.533.2

[Abstract] Microwave discharge in a gas with the microwave field intensity just above the threshold (cutoff) level and thus below the breakdown level is analyzed, considering the case of such a microwave field concentrated within a region smaller than the potential well. The gas is assumed to be a low-pressure atomic one in which charged particles are generated essentially by direct electron-impact ionization of atoms and the frequency $\nu_{en}(\nu_e)$ of elastic electron-atom collisions is much higher than the frequency $\nu_{ec}(\nu_e)$ of elastic electron-electron collisions on an absolute basis but much lower than the latter on a relative basis, i.e., when multiplied by the ratio m/M of electron mass to atom mass. Both frequencies are functions of the electron velocity ν_e , which is replaced by the electron energy $u = m\nu_e^2/2 + e\phi(r)$ (e - electron charge, $\phi(r)$ - potential of constant ambipolar electric field confining electrons within the gas-discharge plasma). The electron distribution function is expanded into a series of spherical harmonics in the velocity space, an equation of kinetics then being obtained for an expanded electron distribution function which is isotropic in that velocity space. The right-hand side of this equation consists of two terms representing electron-electron interaction and electron-(microwave)field interaction respectively. The latter is evaluated, assuming further that the mean electron energy (temperature) does not significantly change with increasing distance from the region of the concentrated microwave field. Electrons with energy lower than the potential barrier and thus remaining within the potential well are considered first. Electrons with energy higher than the potential barrier and thus overcoming it are considered next, of concern being their presence in the region where their energy distribution is appreciably influenced by the microwave field. From the equation of number-of-electrons balance is obtained an expression for the frequency of ionizing electron impacts on atoms. The space distribution of plasma density and that of the ambipolar electric field are obtained from the equation of number-of-particles continuity and the equation of quasi-neutrality. The one-dimensional problem is solved accordingly for calculating the threshold microwave field and the plasma parameters. Its analytical solution is supplemented with a numerical data pertaining to a discharge in argon. The author thanks A. N. Starostin for discussing the results. References 4.

Vortex Entrainment by Magnetostatic Wave in Composite Ferrite and High- T_c Superconductor Structure

917J0024C Leningrad PISMA V ZHURNAL
TEKHNICHESKOY FIZIKI in Russian Vol 16 No 17,
12 Sep 90 pp 73-76

[Article by N. I. Polzikova and A. O. Rayevskiy]

[Abstract] Interaction of a magnetostatic wave and a high- T_c superconductor layer under a ferrite film is analyzed theoretically, experiments having revealed that a spin wave becomes absorbed by superconductor electrons and loses energy with an attendant transfer of its momentum to them. This is shown to result in their entrainment, vortices having already been shown to move in a magnetostatic wave with some average velocity as the field of this wave penetrates into the superconductor layer. The nonlinear relation between the instantaneous velocity of such vortices and the magnetic field intensity, their entrainment being a consequence of this relation, and the existence of vortex clusters which fall into potential wells formed by the nonuniform field of the magnetostatic wave are taken into account. As a model problem is considered a double-layer structure consisting of an yttrium-iron-garnet film on a high- T_c superconductor film or plate and a parallel magnetostatic wave propagating through it, in a normally oriented external magnetic field of an intensity much higher than the lower critical and much lower than the upper critical for this superconductor. The alternating electromagnetic field of the wave induces an alternating current in the superconductor and a Lorentz force acting on the vortices. Inertia and interaction of vortices are ignored, assuming also that the frequency of the wave is much higher than the vortex pinning frequency. The entrainment e.m.f. is calculated on this basis from the laws of energy and momentum conservation, according to G. Weinreich (PHYSICS REVIEW Vol 107 No 1). The expression for this e.m.f. and the dispersion relation in the linear approximation yield an entrainment effect proportional to the phenomenologically defined absorption coefficient, analogous to the acoustoelectric effect in a piezoelectric superconductor. The sensitivity characterizing this effect in a ferrite-superconductor structure is estimated to be within the 0.01 - 0.1 V/W range. The authors thank P. Ye. Zilberman for helpful participation and discussion. Figures 1; references 9.

Thermodynamics of Metal-to-Superconductor Transition

917J0039A Moscow DOKLADY AKADEMII NAUK
SSSR in Russian Vol 314 No 3, Sep 90 pp 609-612

[Article by Academician N. N. Sirota, BSSR Academy of Sciences, Moscow Institute of Hydromelioration]

UDC 538.953

[Abstract] Considering that transition of a metal from normal state to superconducting state involves essentially its electronic subsystem, transition from disordered turbulent and lossy flow of electrons to laminar lossless flow of electron pairs along equipotential lines in many cases being one of the second kind and thus a fuzzy or intermediate one, attendant changes in the Gibbs free energy and in the specific heat are evaluated from the standpoint of the author's geometrothermodynamical "envelope" theory not inconsistently with the Ginzburg-Landau theory and the Goerter-Casimir two-fluid theory. The latter is accordingly modified by adding to the sum $G_{sn} = G_n W_n^\alpha + G_s W_s$ (W_s, W_n - concentrations of "normal" and superconduction electrons respectively, $\alpha < 1$ for phase transitions of the second kind) the mixing interaction energy ΔH_{sn} minus the heat of mixing $T \Delta S_{sn}$. The temperature dependence of that free energy and of the specific heat c_{ns} in intermediate states of the electronic subsystem within the superconducting transition range is then calculated according to this two-fluid model and also in the approximation of quasi-regular solutions with a statistically uniform distribution of "normal" and superconduction electron pairs, the presence of superconducting clusters in the form of domains or filaments being accounted for by an $\alpha < 1/2$ ($\alpha = 1/2$ in the case of random flow of electron pairs). Figures 2; references 7.

Synthesis and Physical Properties of Tl-Ca-Ba-Cu-O High- T_c Superconductors

917J0045A Tomsk IZVESTIYA VYSSHIKH
UCHEBNIKH ZAVEDENIY: FIZIKA in Russian
Vol 33 No 9, Sep 90 pp 18-22

[Article by G. A. Petrakovskiy, V. Ye. Volkov, G. S. Patrin, T. A. Bidman, N. I. Kiselev, and V. N. Vasilyev, Institute of Physics imeni L. V. Kirenskiy, Siberian Department, USSR Academy of Sciences]

UDC 537.312:538.27

[Abstract] An experimental study of high- T_c superconductors in the Tl-Ca-Ba-Cu-O system was made, specimens had been produced under various process conditions from Ca_2CuO_3 , $Ba(NO_3)_2$, and CuO powders, thoroughly mixed at a temperature within 800 - 810°C and then annealed. This procedure was repeated twice, and then again with Tl_2O_3 powder. This time the powders were mixed in alcohol, dried, and then compacted with or without an oxidizer added, whereupon the pellets were annealed at 820°C for 3 - 5 min. Two groups of specimens were thus produced, some with and some without oxidizer added before compaction. Their electrical resistivity was measured by the current-voltage method and their magnetization ($G \cdot cm^3/2$) was measured with a pendulum magnetometer, both over the 77 - 300 K temperature range. Their response to 10.7 GHz microwave excitation was measured by the conventional method in a standard EPR-spectrometer. Their x-ray

diffraction spectra were recorded in a DRON-3 diffractometer with a CuK_α -radiation source. The results of electrical and magnetic measurements indicate that both volume fraction and composition of the superconducting phase are different in Tl-Ca-Ba-Cu-O ceramics produced under different conditions, namely with and without oxidizer respectively. This is confirmed by the x-ray diffraction spectra and the microwave absorption spectra. Considering that microwave absorption by high- T_c superconductor ceramics is associated with the Josephson effect and that it is an ensemble of weak links which evidently couples the superconducting grains here, the microwave response of Tl-Ba-Cu-O ceramic can be interpreted in terms of the superconducting glass model. A diamagnetic susceptibility of ceramic Tl-Ca-Ba-Cu-O was recorded in extremely weak magnetic fields only, weak links evidently being broken and diamagnetism thus being suppressed in stronger magnetic fields. Figures 6; references 6.

Quantum Interference in Tl-Ca-Ba-Cu-O High- T_c Superconductor Ceramics

917J0045B Tomsk IZVESTIYA VYSSHIKH UCHEBNYKH ZAVEDENIY: FIZIKA in Russian Vol 33 No 9, Sep 90 pp 26-29

[Article by D. A. Velikanov, G. S. Patrin, G. A. Petrakovskiy, and V. Ye. Volkov, Institute of Physics imeni L. V. Kirenskiy, Siberian Department, USSR Academy of Sciences]

UDC 537.312.62

[Abstract] The feasibility of using Tl-Ca-Ba-Cu-O ceramics as materials for superconducting quantum interference devices was studied by the experimental method, with the sensing element connected into a standard high-frequency SQUID circuit and placed in a cryostat. Ceramic Tl-Ca-Ba-Cu-O material with a critical superconducting transition temperature $T_c = 115$ K was selected for this study, formed into 8 mm long bars with a 2 mm square cross-section and into rings with a 2.5 mm inside diameter. The rings included a 0.3 mm long weak-link segment with a 0.1 mm square cross-section. Macroscopic quantum interference was recorded in all specimens. Tests were performed at two SQUID-magnetometer operating temperatures T_0 , at 77 K inside a superconducting Nb shield and without one and at 4.2 K without shields. Measurement of the voltage-field characteristic of bars at 77 K revealed a regular but not triangular oscillatory field dependence of the voltage with "particular" periods superposed on the "principal" period. That period differed for different specimens and thus evidently depended on technological factors. Regularity of the voltage-field characteristic indicated a synchronization of circuits, an effective quantization area of the order of 0.001 mm^2 having evidently been attained. The voltage was consistently lower at 4.2 K throughout the 0 - 0.003 G range of magnetic induction, the effective quantization area evidently being smaller as a consequence of either a wide diversity of weak links with

respect to critical current or a multiphase diversity of the material in terms of critical temperature. Measurement of the voltage with a synchronous detector as a function of time, following application of pulsed magnetic field, revealed a rise of the voltage even without a shield at 4.2 K but not without a shield at 77 K. Bars of Tl-Ca-Ba-Cu-O ceramic were found to perform better at 77 K than similar bars of Y-Ba-Cu-O ceramic. Ring interferometers with a thin segment were, moreover, found to have better performance characteristics (a sensitivity of the order of $10 \mu\text{V}$ per flux quantum having been attained with the best specimen) including higher stability than those of bar interferometers and to retain most of the properties of the latter. Figures 3; references 13.

Damon-Eschbach Waves in Ferromagnetic Film With Superconductor Coating

917J0053A Leningrad PISMA V ZHURNAL TEKHNIЧЕСКОY FIZIKI in Russian Vol 16 No 23, 12 Dec 90 pp 27-32

[Article by Yu. I. Bespyatykh, A. D. Simonov, and V. D. Kharitonov, Institute of Radio Engineering and Electronics, USSR Academy of Sciences, Fryazino branch]

[Abstract] The effect of a superconductor coating on the spectrum of surface magnetostatic waves in a ferromagnetic film is analyzed theoretically by considering the interaction of such waves and the vortex structure, in a tangentially oriented external magnetic with an intensity higher than the lower critical and lower than the upper critical for a metal-oxide superconductor. The magnitude of this effect is shown to depend on the thickness of the coating as well as on the direction of wave propagation. Assuming that the contact between the two films in the $y = 0$ plane to be continuous and the Ginzburg-Landau parameter to be $\kappa = \gamma_L/\xi \gg 1$ (γ_L - London penetration depth, ξ - coherence length), the dispersion relation for the frequency of such waves is derived from the equations of magnetostatics and the equation of transient superconductivity theory with the appropriate boundary conditions. Next is considered vibratory motion of vortices in a thin superconductor film, of a thickness much smaller than the coherence length but much larger than the London penetration depth, and the effect of their motion on the spectrum of those surface magnetostatic waves is evaluated accordingly. Inertia and interaction of vortices are ignored, but the alternating electric field induced by moving vortices in the superconductor film is essential. The model equation of motion for a quantum of magnetic flux and the applicable two field equations of magnetostatics yield the dispersion relation $i\xi D_0 - D_m = 0$ (D_0 , D_m referring to surface magnetostatic waves in a ferromagnetic film without superconductor coating and in one coated with a film of an ideal metal respectively). A special case is $k_z = 0$, namely zero tangential component (in the direction of the external magnetic field) of the wave vector. The scattering of surface magnetostatic waves by moving

vortices is for this case evaluated in terms of the coefficient of resulting wave self-transformation and its dependence on the intensity of the tangential magnetizing field as well as on the magnitude of the Ginzburg-Landau parameter. Numerical calculations have been made with $\kappa = 5, 10, 15, 20$. The dispersion relation for the frequency of surface magnetostatic waves on a ferromagnet coated with a film of a type-2 superconductor is compared with that in the two opposite limiting cases of a ferromagnet coated with a film of an ideal metal and a ferromagnet under vacuum. The authors thank A. V. Vashkovskiy for interest. Figures 2; references 7.

Phonon Mechanism of Superconductivity in Strongly Correlated Systems

917J0057C Moscow PISMA V ZHURNAL
EKSPERIMENTALNOY I TEORETICHESKOY
FIZIKI in Russian Vol 53 No 1, 10 Jan 91 pp 21-23

[Article by A. O. Anokhin, V. Yu. Irkhin, and M. I. Katsnelson, Institute of Metal Physics, Ural Department, USSR Academy of Sciences, Sverdlovsk]

[Abstract] The electron-phonon interaction mechanism of singlet pairing in strongly correlated systems such as

high- T_c superconductors is analyzed by the method of Green's function, with electron-electron interaction in the normal phase included exactly but its contribution to the anomalous part of Green's function disregarded. The expression for the critical superconducting transition temperature obtained from the two Eliashberg equations for $\chi_k(ip_n)$ and $\phi_k(ip_n)$ in the approximation of weak electron-phonon coupling indicates no renormalization of electron-phonon interaction in the Fermi-liquid model even where "heavy fermions" are involved, at least in the adiabatic case. In the marginal Fermi-liquid model weak electron-phonon interaction is shown to lower the critical temperature, while in the Anderson model "infrared catastrophe" or Van Hove singularities are shown to raise it. In the "Hubbard-III" approximation electron-phonon interaction leads to electron-electron repulsion and strong decay of electronic states at the Fermi level so that in the Hubbard model of metal-to-insulator transition, where the Fermi-liquid theory is invalid, superconducting transition cannot occur above the critical Hubbard repulsion potential. The role of electron-phonon interaction in superconductivity is thus subject to different interpretations, depending on the accepted model of the normal phase. References 7.

**Effect of Temperature Gradient on
Thermodynamic and Correlation Characteristics of
Nonhomogeneous Substance Near Critical Point**

917J0055C Kiev UKRAINSKIY FIZICHESKIY
ZHURNAL in Russian Vol 35 No 12, Dec 90
pp 1827-1830

[Article by A. D. Alekhin and L. A. Bulavin, Kiev
University imeni T. G. Shevchenko]

UDC 536.532

[Abstract] A substance in the vicinity of the critical point is considered, its altitudinal nonhomogeneity here being caused by the vertical gradient of the chemical potential and that of its fluctuation part. The effect of a positive vertical temperature gradient on those and other profiles of a substance in this state is analyzed according to the fluctuation theory of phase transitions and using thermodynamic similarity. While the compressibility of a substance increases abruptly during evaporation, existence of a vertical temperature is shown not to influence it at the altitude where the vertical gradient of static pressure $\Delta h/\Delta z = \rho_c g/P_c = 0$ (ρ_c - density of substance at critical point, P_c - critical pressure, T_c - critical temperature, Δz - altitude above level where density is $\rho = \rho_c$ when $T > T_c$, near the critical isochore, or above

interphase boundary when $T < T_c$). The altitudinal density profile is shown to be different, the amplitude of the vertical density gradient depending on the vertical temperature gradient as well as on the vertical gradient of the fluctuation part of the chemical potential. In the thermodynamic direction, close to the critical isotherm, a vertical temperature gradient is shown to have no effect on the nonhomogeneity of a substance, its nonhomogeneity being determined solely by its critical temperature. These conclusions are confirmed by experimental data on a binary solution CO_2 - ^4He , measurements having been made by passage of slow neutrons. The asymmetry of the altitudinal density, compressibility, and correlation radius profiles of substances with a critical temperature far above 126 K indicates that the vertical gradient of the chemical potential is in the case of such a substance much smaller than that of its fluctuation part. The effect of a vertical density gradient and thus of gravity on the altitudinal profile of the chemical potential in the vicinity of the critical point was also measured by passage of slow neutrons, in an experiment with a binary solution CO_2 - C_2H_6 . For this measurement the mixture was held in a container 20 cm high with a 5 cm wide base. The effect of a vertical temperature gradient on that profile was then measured with the container turned down so as to be 5 cm high with a 20 cm wide base. Figures 1; references 12.

Fluctuation Spectrum in Exactly Solvable Model With Dissipation: New Model of Flicker Noise

917J0052A Tomsk IZVESTIYA VYSSHIKH
UCHEBNIKH ZAVEDENIY: FIZIKA in Russian
Vol 33 No 10, Oct 90 pp 13-18

[Article by O. Yu. Dinariyev, All-Union Scientific
Research Institute of Natural Gas]

UDC 538.56+530.145

[Abstract] Fluctuations of a quantum oscillator interacting with a field in the ambient medium and decaying because of attendant dissipation are considered, this model had been made exactly solvable by stipulation of a quadratic Lagrangian, owing to the consequent linearity of its equations of dynamics. The spectral function of its quantum and thermal fluctuations can therefore be calculated directly, which is done in a system of units with both Planck and Boltzmann constants made equal to one. Calculations are based on the Hamiltonian of this "oscillator-field" system, assuming also that the sufficient and necessary condition $\gamma = 1 - \int_0^\infty q^2 \omega^{-2} d\omega > 0$ (ω - frequency, $q(\omega)$ - weight function) for positive-definiteness of the Hamiltonian is satisfied so that the system remains energetically stable. The corresponding Hamilton equations describing the system dynamics are obtained from that Hamiltonian and the symplectic form. Canonical quantization of the model Lagrangian, upon standard introduction of generation-annihilation operators and postulation of commutative laws, yields both the quantum time correlation function $B(t)$ and the spectral density $B(\omega)$ of oscillator fluctuations. The latter for the dissipative case is also obtained by application of the Callen-Welton theorem. The low-frequency range of the fluctuation spectrum is then characterized by a spectral density $B(\omega) = \pi C^2 \gamma^{-2} \beta^{-1} |\omega|^{-1+\varepsilon}$ form (C - constant, β - inverse temperature, $0 < \varepsilon < 1$), which can be regarded as another model of flicker noise and which becomes $B(\omega) = (\pi C^2 \beta)^{-1} [\cos \pi(1 + \varepsilon)2] |\omega|^{-1-\varepsilon}$ as the stability limit is approached ($\gamma \rightarrow 0$).

Mechanism of P- and CP-Invariance Violation in Nonassociative Field Theory

917J0052B Tomsk IZVESTIYA VYSSHIKH
UCHEBNIKH ZAVEDENIY: FIZIKA in Russian
Vol 33 No 10, Oct 90 pp 92-97

[Article by D. F. Kurdgelaidze and G. A. Begeluri, Tbilisi University]

UDC 530.145:530.12:537.8

[Abstract] A new quantum number having been introduced by the nonassociative classical octonion spinor field theory having, namely, the associator as measure of nonassociativeness and also as a partner of the spin, it is now possible to classify particles and antiparticles with respect to both associator and spin. Inasmuch as the associator is also the eigenvalue of the Lorentz group generator, their physical states can be classified accordingly and spin-associator interaction as a kind of weak interaction may be introduced. A new kind of such an interaction, an analog of ultraweak ones, is introduced here which describes nonconservation of P-parity in some processes and of CP-parity in others. Considering first that the nonassociative theory assigns not only a spin but also an associator $1/2$ or 1 respectively to quark, lepton, and intermediate boson states, but no associator to the γ -photon and the Z_0 -boson, it is then presumed that weak interactions obey superselection rules which preclude associator conservation. Several specific examples with available experimental data demonstrate that associator changes $|\Delta A| = 1$ and $|\Delta A| = 2$ correspond to violation of P-parity and CP-parity respectively, examples of P-parity violation being β -decay of $^{60}\text{Co}_{27} \rightarrow ^{60}\text{Ni}_{28} + e^- + \bar{\nu}_e$ (net spin change $|\Delta S| = 0$) and $\pi^+ \rightarrow e^+ + \bar{\nu}_e$ ($\bar{\nu}_e$ with an attendant associator change $|\Delta A| = 1$). The only so far known examples of CP-invariance violation are decays of long-lived neutral K-mesons: $K_L^0 \rightarrow \pi^+ \pi^-$, $K_L^0 \rightarrow \pi^0 \pi^0$, $K_L^0 \rightarrow e^+ \pi^- \pi^+ \text{gn}_e(\bar{\nu}_e)$, $K_L^0 \rightarrow \mu^+ \pi^- \pi^0$ ($\pi^0 \rightarrow \mu^+ \mu^-$), also $K^0 \rightarrow K^0$ and $K^0 \rightarrow K^0$ conversions. The validity of superselection rules being thus confirmed, diagrammatically as well as experimentally, $K_L^0 \rightarrow \mu^+ \mu^-$ decay may very well be another case of CP-invariance violation in accordance with those rules. No experimental data on this process are available and CP-violation in this case is, moreover, not experimentally verifiable with existing means. Figures 4; references 10.

NTIS
ATTN: PROCESS 103
5285 PORT ROYAL RD
SPRINGFIELD, VA

2

22161

This is a U.S. Government publication. Its contents in no way represent the policies, views, or attitudes of the U.S. Government. Users of this publication may cite FBIS or JPRS provided they do so in a manner clearly identifying them as the secondary source.

Foreign Broadcast Information Service (FBIS) and Joint Publications Research Service (JPRS) publications contain political, military, economic, environmental, and sociological news, commentary, and other information, as well as scientific and technical data and reports. All information has been obtained from foreign radio and television broadcasts, news agency transmissions, newspapers, books, and periodicals. Items generally are processed from the first or best available sources. It should not be inferred that they have been disseminated only in the medium, in the language, or to the area indicated. Items from foreign language sources are translated; those from English-language sources are transcribed. Except for excluding certain diacritics, FBIS renders personal and place-names in accordance with the romanization systems approved for U.S. Government publications by the U.S. Board of Geographic Names.

Headlines, editorial reports, and material enclosed in brackets [] are supplied by FBIS/JPRS. Processing indicators such as [Text] or [Excerpts] in the first line of each item indicate how the information was processed from the original. Unfamiliar names rendered phonetically are enclosed in parentheses. Words or names preceded by a question mark and enclosed in parentheses were not clear from the original source but have been supplied as appropriate to the context. Other unattributed parenthetical notes within the body of an item originate with the source. Times within items are as given by the source. Passages in boldface or italics are as published.

SUBSCRIPTION/PROCUREMENT INFORMATION

The FBIS DAILY REPORT contains current news and information and is published Monday through Friday in eight volumes: China, East Europe, Soviet Union, East Asia, Near East & South Asia, Sub-Saharan Africa, Latin America, and West Europe. Supplements to the DAILY REPORTs may also be available periodically and will be distributed to regular DAILY REPORT subscribers. JPRS publications, which include approximately 50 regional, worldwide, and topical reports, generally contain less time-sensitive information and are published periodically.

Current DAILY REPORTs and JPRS publications are listed in *Government Reports Announcements* issued semimonthly by the National Technical Information Service (NTIS), 5285 Port Royal Road, Springfield, Virginia 22161 and the *Monthly Catalog of U.S. Government Publications* issued by the Superintendent of Documents, U.S. Government Printing Office, Washington, D.C. 20402.

The public may subscribe to either hardcover or microfiche versions of the DAILY REPORTs and JPRS publications through NTIS at the above address or by calling (703) 487-4630. Subscription rates will be

provided by NTIS upon request. Subscriptions are available outside the United States from NTIS or appointed foreign dealers. New subscribers should expect a 30-day delay in receipt of the first issue.

U.S. Government offices may obtain subscriptions to the DAILY REPORTs or JPRS publications (hardcover or microfiche) at no charge through their sponsoring organizations. For additional information or assistance, call FBIS, (202) 338-6735, or write to P.O. Box 2604, Washington, D.C. 20013. Department of Defense consumers are required to submit requests through appropriate command validation channels to DIA, RTS-2C, Washington, D.C. 20301. (Telephone: (202) 373-3771, Autovon: 243-3771.)

Back issues or single copies of the DAILY REPORTs and JPRS publications are not available. Both the DAILY REPORTs and the JPRS publications are on file for public reference at the Library of Congress and at many Federal Depository Libraries. Reference copies may also be seen at many public and university libraries throughout the United States.